Summer 7-30-2018

CHARACTERIZATION OF GALLIUM NITRIDE PHOTOCONDUCTIVE SEMICONDUCTOR SWITCHES IN THE NONLINEAR REGIME

Joseph D. Teague
University of New Mexico - Main Campus

Joseph D. Teague
Candidate

Electrical and Computer Engineering
Department

This thesis is approved, and it is acceptable in quality and form for publication:

Approved by the Thesis Committee:

Jane Lehr, PhD — Chairperson

Salvador Portillo, PhD

Olga Lavrova, PhD

CHARACTERIZATION OF GALLIUM NITRIDE PHOTOCONDUCTIVE SEMICONDUCTOR SWITCHES IN THE NONLINEAR REGIME

by

JOSEPH D. TEAGUE

BACHELOR OF SCIENCE, ELECTRICAL ENGINEERING
ROSE-HULMAN INSTITUTE OF TECHNOLOGY, 2011

THESIS

Submitted in Partial Fulfillment of the
Requirements for the Degree of

Masters of Science
Electrical Engineering

The University of New Mexico
Albuquerque, New Mexico

December, 2018

ACKNOWLEDGEMENTS

I could not have done this without the love and support of my family and friends, particularly my wife Miriam Maestas. I'd also like to thank my employer - the Air Force Research Laboratory, Directed Energy Directorate - as well as Sandia National Laboratories for trusting me and giving me this opportunity. Additional thanks to Dr. Jane Lehr, Dr. Fred Zutavern, Dr. Salvador Portillo, Dr. Olga Lavrova, Dr. Alan Mar, Emily Hirsch, Richard Gallegos, Verle Bigman, Mike Van Heukelom, Greg Pickrell, and Joshua Atencio for their time, energy, and patience with me on this project. I owe you all a debt of gratitude which hopefully I can repay someday.

CHARACTERIZATION OF GALLIUM NITRIDE PHOTOCONDUCTIVE SEMICONDUCTOR SWITCHES IN THE NONLINEAR REGIME

by

Joseph D. Teague

B.S., Electrical Engineering, Rose-Hulman Institute of Technology, 2011

M.S., Electrical Engineering, University of New Mexico, 2018

ABSTRACT

The energy demands of an increasingly electrified world have caused a renewed interest in once dormant fields of research. Photoconductive Semiconductor switches (PCSS) are one of these fields. They theoretically offer high voltage, high current switching in sub cm^3 packaging, without the shot to shot variation and bulk of current high-power DC switches such as spark gaps. PCSS are capable of power densities of 10^9-10^{10} W/cm^3, with electric fields ranging from 10^5-10^6 V/cm and current densities from 10^4-10^6 A/cm^2 [1].

Most PCSS make a trade-off between voltage, current, and durability, which make them unsuitable for applications which require all three. GaN PCSS appear to offer the most potential, combining high hold-off voltages with high repetition rates and current handling capability. However, it is only recently that fabrication of GaN has reached a maturity level suitable for PCSS research and as a result they are not as well characterized as PCSS utilizing GaAs or SiC. The theoretical performance of GaN PCSS is greater than that of other materials, particularly if GaN can be shown to have a nonlinear mode of operation, reducing laser power needed to trigger the device.

Along with an in-depth characterization, the potential existence of a "high-gain" mode of operation in optically triggered GaN solid-state lateral switches across a variety of voltages, triggering wavelengths, and triggering energies is examined.

TABLE OF CONTENTS

Chapter 1:

1.1: Introduction to PCSS

The interaction between solid material and light has long been known. The quantum link between conduction bands of metals and photon wavelength was first described by Einstein. In semiconductors, where the photon energy to cause conduction by carrier transition is small and easily achieved, the phenomena may be used as a light activated switch. In general, light activated switches are known as photoswitches. A specific class of photoswitches, known as photoconductive semiconductor switches (PCSS).

PCSS are optically triggered switches capable of rise times less than 300ps and switch frequencies ranging from Hz to MHz [2] [3]. The prospect of a small, high-frequency, high power solid-state switch allows for a design space that complements and potentially replaces spark gaps and high-power IGBTs. The combination of high power and high-frequency makes these switches of interest to both the pulsed power community and DC/DC converter community as they allow for more space and energy-efficient high-power converters and pulsed power sources.

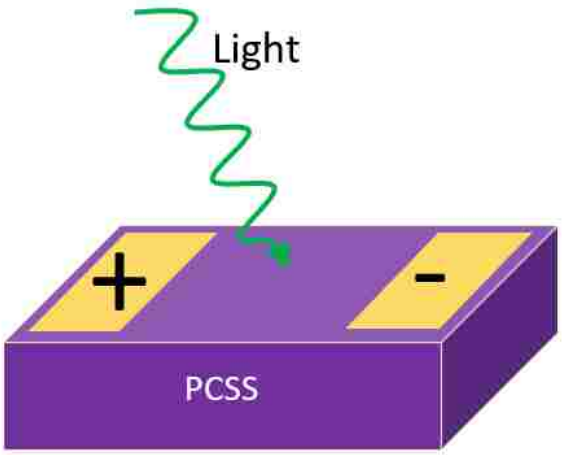

Figure 1: Example of a Lateral PCSS. Gold is the contacts, purple is the bulk semiconductor material of the PCSS

The voltage a device can handle for a given size is determined in a large part by its bandgap. In semiconductor devices, bandgap is used to refer to the necessary energy level (often stated in electron volts) needed to move electrons in the device from the valence band to the conduction band. This movement of electrons to the conduction band is what makes the device conduct electricity when in an "on" state. The bandgap and other material properties for four of the primary materials used in PCSS research are shown in Table 1.

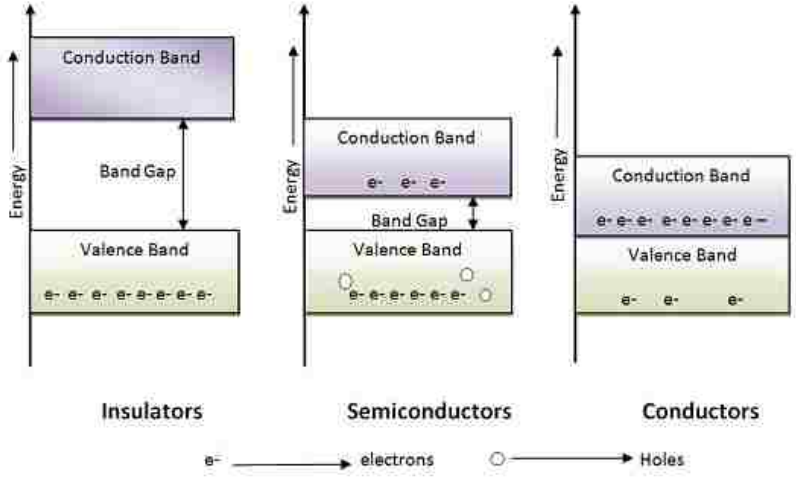

Figure 2: Schematic Diagram showing relative bandgap differences between insulators, semiconductors, and conductors [4]

Properties	Si	GaAs	4H-SiC	GaN
Bandgap (eV)	1.11	1.43	3.26	3.42
Dielectric constant	11.8	12.8	9.7	9
Breakdown Field (MV/cm)	0.25	0.35	3.5	3.5
Thermal Conductivity (W/cm°K)	1.5	0.46	4.9	1.7

Table 1: PCSS Material Properties

Work on PCSS dates to the 1970s, with most research being focused on silicon as that was and is the most mature PCSS material. In recent decades, other materials have arisen, such as Silicon Carbide (SiC), Gallium Arsenide (GaAs), and Gallium Nitride (GaN) [1].

High voltage PCSS switches being actively pursued are wide-bandgap semiconductors, such as SiC, GaAs, or GaN which are made to be semi-insulating through the addition of impurities, such as vanadium, magnesium, iron, or others. These impurities then form deep acceptors sites within the material. When photons of sufficient energy impact the material, the material becomes conductive due to the excitation of electrons trapped in the deep acceptors into the conduction band [1] [5] [6]. As a result, the device performs analogous to a switch, going from an insulated “off” state, to a conductive “on” state.

These PCSS operate in two separate modes known as “linear” and “nonlinear” (also known as high-gain or “lock-on”). The linear mode is so called because current is directly proportional to optical energy, i.e. each photon generates one electron-hole pair in the device. Any semiconductor will exhibit linear photoconductivity when stimulated at the correct wavelength. The downside to this linear mode is that the optical trigger energies required for switch operation reduce system efficiency and greatly increase

overall system footprint. A less common mode, to date only observed in GaAs and InP, is the high-gain mode, where the device stays conductive beyond the duration of the light pulse and remains so until the electric field across the device drops below a material and light energy dependent threshold [7].

1.2: Advantages of Wide Bandgap Semiconductors

Wide bandgap semiconductors are emerging materials for conventional electronics due to their advantage in power density, high frequency, and high temperature operation over Si or Ge devices. For example, at 3.3eV, SiC has triple the bandgap of Si, which most conventional transistors are made of. This allows it to handle far more voltage and current for a given geometry, as the higher bandgap means more energy is required to force the electrons into the conduction band. Dating back to 1993, research showed that SiC based MOSFETS could be $1/20^{th}$ the size of conventional Si devices operating at the same voltage and current because of this characteristic [8]. On the temperature side, SiC and GaN devices have been tested and operated above 300C on a regular basis, well beyond the 100C limit of Si-based devices, in large part due to their better thermal properties [9]. As a result, they represent the future of power electronics, and multiple studies done on their comparison to Si based devices in the size, weight, and power trade spaces have repeatedly proven that WBG devices offer substantial performance and packaging advantages over current state-of-the-art Si MOSFETS [9] [10] [11]. Similarly, extensive research is being done in these same materials for PCSS devices.

In addition to the higher voltage potential they possess, these wide bandgap semiconductors also possess a higher breakdown field than materials like Si and GaAs. As on-state resistance is inversely proportional to the cube of its breakdown strength, this means wide bandgap materials possess a lower on-state resistance, allowing them to pass much higher currents at a given voltage.

$$R_{on} = \frac{4 \cdot V_{BR}^2}{\varepsilon_r \cdot \mu \cdot (E_c)^3}$$

Equation 1: On-state resistance as a function of breakdown field and breakdown voltage [12]

Multiple "all-in-one" methods of determining the suitability of a semiconductor for operation in a given regime have been derived [12]. Johnson's Figure of Merit (JFOM) applies to high power, high frequency operations. Baliga's FOM (BFOM) is used for low frequency power switching. Baliga's High Frequency FOM (BHFFOM) is used for high frequency power switching. Combined FOM (CFOM) accounts for high temperature, high frequency, and high-power performance. In general, these FOMs are benchmarked to Si as a baseline, having a value of 1. Table 2 and Figure 3 show that in most applications, wide-bandgap materials such as SiC and GaN vastly outperform Si and GaAs.

Property	Si	GaAs	SiC	GaN
JFOM	1	2	324-400	270-480
BFOM	1	13	6-12	17-34
BHFFOM	1	10	57-76	86-172
CFOM	1	4	275-310	108-290

Table 2: Assorted FOM for PCSS Materials

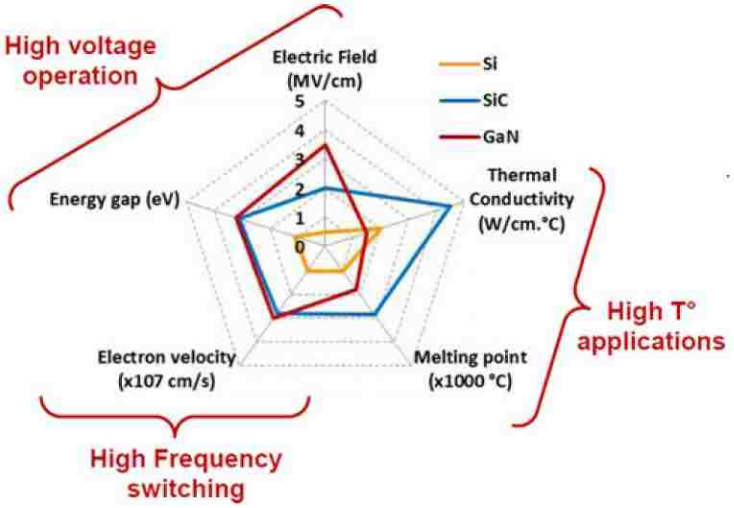

Figure 3: Radar chart comparing Si, SiC, and GaN [12]

1.3: Extrinsic versus Intrinsic Triggering

When it comes to triggering PCSS, while the most obvious choice is to do so at or above bandgap energy (the intrinsic mode), this presents two issues stemming from the same phenomenon. In many materials, absorption increases greatly at and above the bandgap energy. This causes most of the photons to be absorbed in the first few microns of material. As a result, a disproportionate amount of energy is carried across the surface of the device through current crowding and surface flashover. Current crowding is a phenomenon in which current density exceeds the physical limits of the material. Surface flashover is a condition in which the optical trigger induces flashover across the surface of the device, rather than conduction through the device itself. Both these behaviours lead to premature device breakdown and failure [5] [13] [14]. For these reasons, operating in the intrinsic mode is sub-optimal.

Thus, from a device standpoint it is desirable to instead operate sub-bandgap, relying on excitation of the electrons trapped within the impurities/defects of the device

(the extrinsic mode). This allows for the use of wavelengths that penetrate deeper into the device without being absorbed, and thereby utilizing the entirety of the device for current transport. Additionally, this allows the creation of vertical devices such as in Figure 4 instead, as the light can penetrate the bulk of the material, which allows leveraging the bulk properties of the material. This is desirable as it avoids the field enhancement issues inherent in a lateral device due to the electrode/bulk/dielectric triple point. Additionally, vertical devices are anticipated to be easier to shield and have reduced EMI/EMC concerns due to their geometry. However, operating sub-bandgap has the shortcoming of requiring more optical energy, as there are far fewer electrons trapped in the impurities as opposed to the rest of the material. [5]. [1]

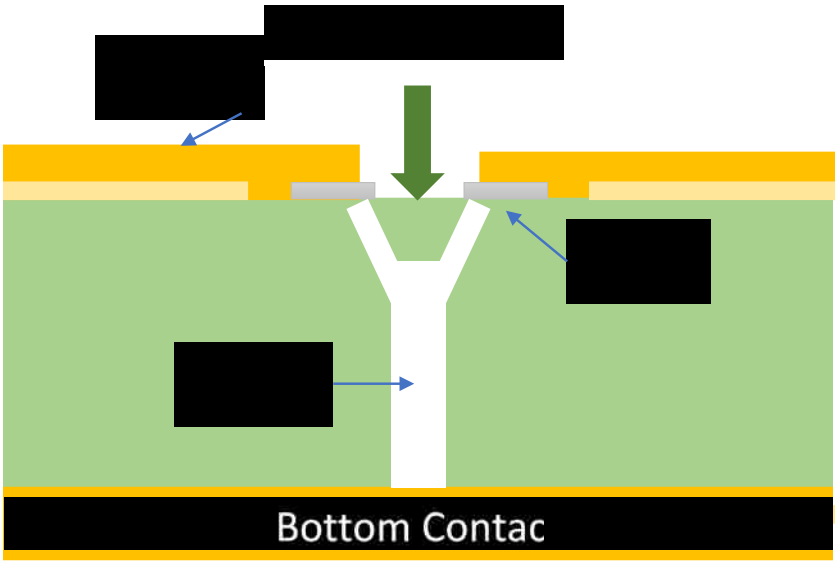

Figure 4: Side view of a vertical PCSS

Another benefit of operating sub-bandgap, is that for wide bandgap materials such as SiC and GaN, finding a cost-effective laser driver becomes much easier. As

[1] Chapter 2 of *Wide Bandgap Extrinsic Photoconductive Switches* by JS Sullivan provides a comprehensive yet concise explanation and overview of the physics of both the linear and nonlinear modes of operation for several different PCSS materials.

wavelength is inversely proportional to bandgap, the higher the bandgap, the smaller the wavelength. This means that higher energy photons can be used without encountering the increased absorption inherent in materials at or above bandgap energy. One example of this is ND: YAG, which is widely available frequency doubled at 532nm (2.34 eV, well below bandgap for both materials, which is greater than 3.2eV). This removes one of the primary barriers to widespread use of PCSS, as it allows for the use of a common commercial wavelength [13]. The lower the bandgap wavelength, the greater the range of laser sources which can be leveraged for sub-bandgap triggering, as can be seen in Figure 5. While commercial viability may not be a research priority for these materials from an academic standpoint, it is critical for the overall development and eventual mass utilization of these devices.

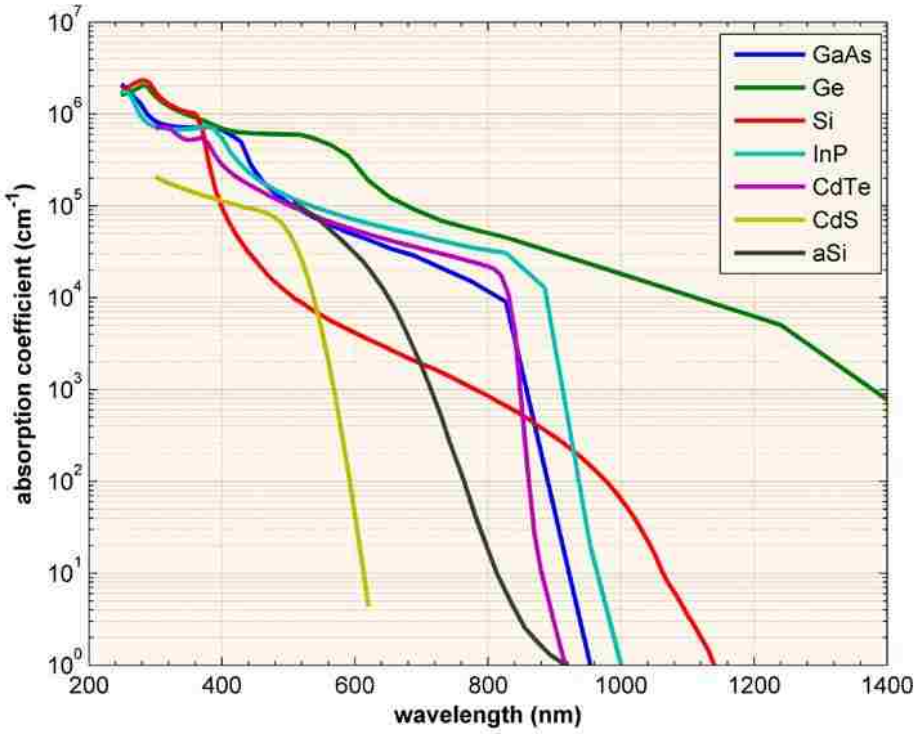

Figure 5: Absorbance vs Wavelength of several semiconductors. CdS, which has the highest bandgap shown at 2.46eV, thus also has the largest range of wavelengths at which it is not absorptive. Ge, which has a bandgap of 0.66eV, is absorptive at all wavelengths shown [15]

Material	Bandgap (eV)	λ (nm)
Si	1.1	1127
GaAs	1.4	885
SiC	3.3	376
GaN	3.4	365
AlN	6.0	207

Table 3: Bandgap vs Wavelength

1.4: Varieties of PCSS and Their Pros/Cons

SiC in the linear mode has had substantial research conducted and is better understood and characterized than other PCSS materials. It also has the best thermal conductivity of the materials commonly studied (beneficial for steady-state operation and cooling) and matches well with existing laser trigger sources. When tested with an ND:Yag laser at 532 and 1064 nm, it exhibited relatively low on-state resistances of 2-3Ω and 11 Ω respectively for 6H-SiC across a 400 micron gap [5]. However, due to its lower drift velocity (and thus maximum current capability), it doesn't have the same high-power potential as GaN and SiC's dark leakage current limits its hold-off voltage compared to GaAs [16]. Moreover, SiC is indirect bandgap, which means it does not absorb light as efficiently as a direct bandgap semiconductor would, and thus requires a larger laser source. It also lacks a high-gain mode, which means the laser trigger must scale directly with the current needed for a given application. As a result, it is not suitable for mobile or space and power constrained applications. However, due to its exceptional high-temperature performance, it is still a material of interest for some niche applications.

GaAs is another popular PCSS material because it has less issue with leakage current than GaN and SiC, as it does have a higher dielectric strength [16], while still having high withstand-voltage and short rise-times. Additionally, because it is a direct

bandgap semiconductor, it is far more efficient at absorbing light near bandgap than Si or SiC, which obviates optical energy requirements. It is the also one of only two materials that have displayed a high-gain, nonlinear “lock-on” mode of operation. However, GaAs was found to have a very limited lifespan at high powers due to its lack of durability, and thus isn’t suited for long-service or high repetition rate applications (lasting less than 350 shots at 14.3kV/cm and 400A) [17].There are methods to improve lifespan by creating more current carrying filaments and thus distributing the load, but these substantially increase optical energy requirements as well as delivery mechanism complexity [2] [18]. Additionally, GaAs has a low optical damage threshold, making it unsuitable for ultrashort pulse systems, as the peak intensities of the laser are high enough to damage the substrate. Our team encountered this firsthand, accidentally destroying a GaAs device we had planned on using for comparative purposes.

“Lock-on” in GaAs was first observed in 1987 by researchers at Sandia National Laboratories [19]. This new phenomenon allowed for switching much higher currents at much lower optical input energies than the linear mode. The lock-on (so-called because the device stays switched into an “on” state after the laser pulse turns off) is characterized by a small linear response to the laser pulse, followed shortly thereafter (anywhere from 350ps to 100ns depending on the switch/optical trigger setup) by a large nonlinear pulse of current that lasts until the voltage across the device drops beneath the lock-on threshold. This high-gain mode is also notable for the formation of filamentary current channels across the device, such as Figure 6, from [7]. The discoverers of this mode state “We believe that current filaments are fundamental to high-gain PCSS and we have never observed high-gain without current filaments.” [7] This observation will be of import

later, as evidence of filamentation will be one of the criteria for the existence of a high-gain mode in GaN.

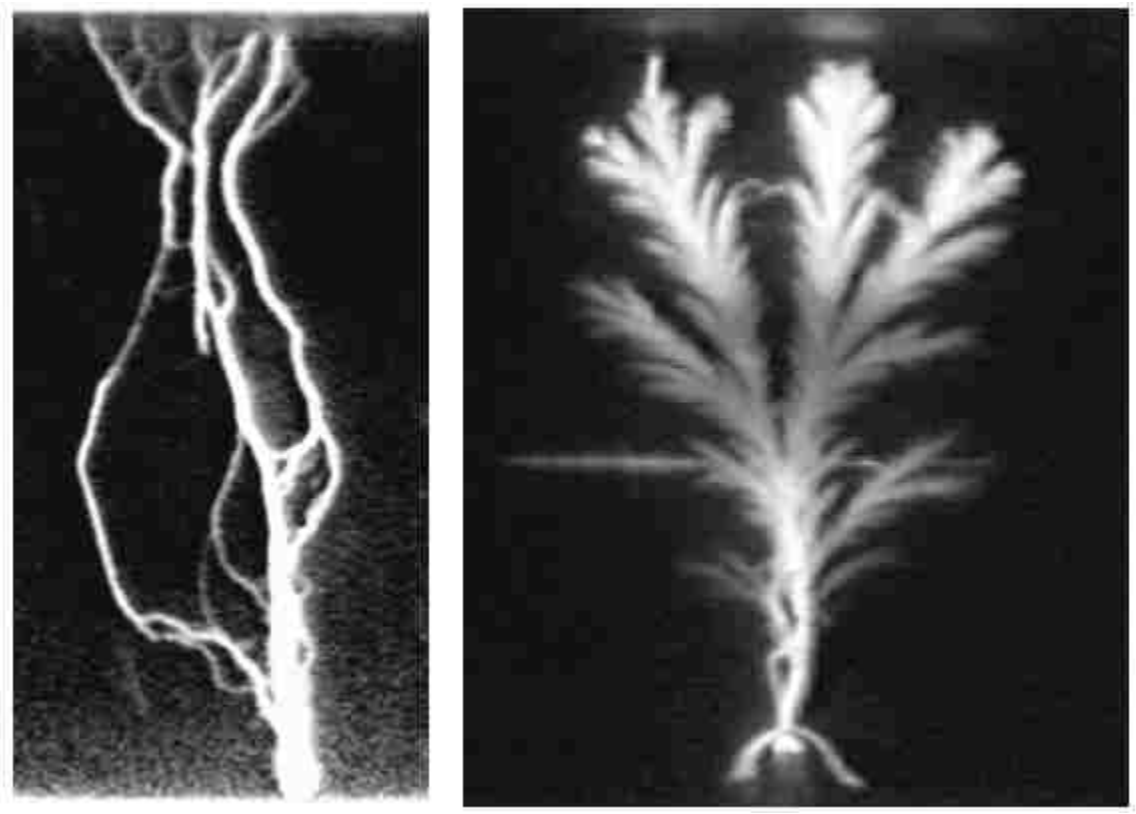

Figure 6: Examples of current carrying filaments from work by Loubriel et al [7]

In this nonlinear mode, each photon generates more than one, often as many as 10^5 electron-hole pairs, enabling tremendous current carrying capability with minimal optical input energy [20]. However, this mode is due to bulk avalanche generation and the switch cannot be turned off until the electric field decreases below the “lock-on” threshold for a given material. While undesirable from a continuous use standpoint, this behaviour is perfectly suited for pulsed applications, where large amounts of power need to be delivered in exceptionally short periods of time, and repetition rates are in the kHz at most, but higher rates are desired. The greatest benefit of this mode is the reduced optical energy required to deliver a given current. The reduction in optical energy (from

mJ to nJ) greatly aids these devices from a systemic standpoint, as one of their primary drawbacks (the bulk of the laser needed to switch the device) is reduced.

This “lock-on” allows these devices to conduct large amounts of current (multiple kA) through small (0.5cm gap) devices at 100+kV with only nJ of laser energy needed to trigger them. Unfortunately, GaAs does not exhibit good durability due to low damage thresholds both electrically and optically. At these power levels, control and design of the incoming optical trigger-such as with line emitting lasers or optical beam splitters- is necessary to achieve high currents without damaging the device. [2] [17] [18]. As such, GaAs in the nonlinear mode is not commercially viable or suitable for continuous operation now and may not be for years to come.

GaN has a higher photoconductive gain than other materials and has a higher volumetric heat capacity, which for high intensity pulsed power applications is critical from a system size and cooling perspective. In addition, GaN is optically triggered and exhibits low resistivity at 532nm, a low-cost and widely commercially available laser wavelength [5] [14]. These aspects make it attractive for size, weight, and power (SWaP) constrained fields such as air or space-based platforms. However, to achieve low on-resistance, the optical trigger needs to be relatively high in intensity, at least partially due to the choice to operate sub-bandgap as mentioned in Section 1.3 [14].

While GaN is attractive for pulsed power due to the superiority of its physical properties relative to GaAs and SiC, it is immature technically. Conventional GaN devices have suffered from poor performance and low yield rates due to difficulty growing and processing the bulk material. Additionally, current generation GaN PCSS

devices do not exceed 250kV/cm hold-off voltages, far short of theoretical limits, which should be greater than 2MV/cm based on the physical properties of GaN [21]. Recent work has been done in the field of linear PCSS devices showing that a novel PCSS architecture resolves the issue of voltage hold-off [16]. Insulated gate PCSS, in which a traditional MISFET is used in series with the PCSS, utilizes a traditional transistor to keep the switch "off". However, by using the PCSS in series with a traditional transistor, switching frequency and current carrying capability is limited to that of the traditional device. Additionally, to date, GaN has not been shown to possess a nonlinear mode like that of GaAs or InP.

As the bulk GaN procured for this project was obtained from two manufacturers, Kyma and AMMONO, the literature search focused on experiments performed using GaN from these two manufacturers [22] [23]. This would allow direct comparison between previous results and the results of this project.

Sullivan conducted extensive research into both SiC and GaN PCSS switches for Lawrence Livermore National Laboratories. His work in GaN involved testing a vertical device using GaN made by Kyma, one of the two primary manufacturers of bulk GaN used for PCSS. This device was tested at 1064nm with negligible response, as well as at 532nm using a 5.5ns, 0.5-12mJ pulse with a bias voltage of 1000V across a 400 micron gap. While his work did show that GaN exhibits an excellent response at that wavelength, with conductivity increasing as the square of peak optical power (to 0.7 Ω resistance at 12mJ), no operation outside of the linear mode was demonstrated. However, a nonlinear operation was not the focus of his research, but rather a characterization and comparison of SiC and GaN in the linear mode when triggered using a 532nm source [5].

In 2013, Leach published the results of some efforts made by Kyma Technologies in developing high voltage, high current GaN PCSS devices. The device was an edge illuminated PCSS as shown in Figure 7. These results also were obtained using a 532nm laser source, with optical energies of 0 (purely off-state) to 0.6mJ and pulse widths ranging from 160ps to 5.5ns. This work showed again the suitability of 532nm sources in switching GaN PCSS. On-state resistance was less than 1 Ω at energies above 0.6 mJ. These results were superior to Sullivan's, but the switch geometry was different, and the material was from a different batch. Because GaN processes are less developed than those of other semiconductor materials, there can be substantial batch to batch variation in dopant concentrations and thus off and on-state resistivity. This can lead to disparities in results, as is seen here. Again however, no evidence of nonlinear behaviour was observed, and obtaining evidence of this was not the primary goal of the research [14].

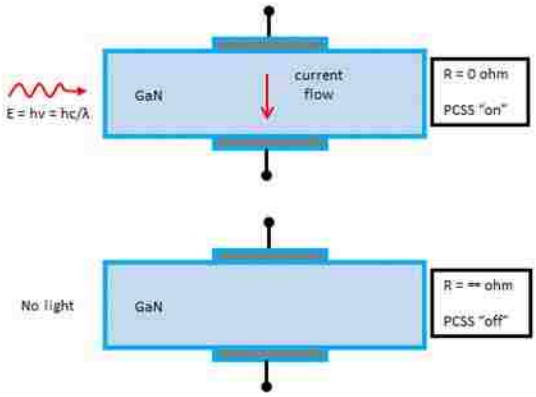

Figure 7: Kyma GaN PCSS Schematic from [14]

An effort was also made by Texas Tech University to leverage recent advances in GaN material quality to test different device and electrode geometries. This was done to see if nonlinear behaviour could be observed while triggering GaN PCSS near bandgap at 355nm. The effort used GaN made by both Kyma and AMMONO, which made it a

directly applicable to the work planned for this thesis, as those were the two vendors providing material to this project as well. Both lateral and vertical geometries were tested at field strengths up to 200kV/cm, with laser fluence of 4mJ/cm^2 (0.26 mJ total to the lateral devices, 4mJ to the vertical) and pulse width of ~8ns. Despite testing multiple devices at a variety of field strengths, no evidence for any nonlinear operation was found. However, they believe modifications to both electrodes and substrate geometry may allow for the discovery of a nonlinear mode [24].

If a material can be found that exhibits both "lock-on" and durability at high powers without requiring large amounts of laser input energy to trigger it, there will be a robust academic and military demand for it. To date however, no such material has been found.

1.5: Results of the Literature Review

To date there has been no research demonstrating nonlinear phenomena in GaN. However, it was beneficial to examine the properties of PCSS in general, particularly work done in the linear mode in GaN by Kyma, one of the suppliers of bulk GaN for this project. It was also useful to examine the literature on GaAs in the nonlinear mode so that the performance of GaN devices (if a nonlinear mode was present) could be compared to a more mature, well researched technology.

Author	Vendor	Geometry	Gap	λ (nm)	Trigger (mJ)	V (kV)	E (kV/cm)	Mode
Sullivan	Kyma	Vertical	400 μm	532	12	1	25	Linear
Leach	Kyma	Vertical	400 μm	532	5	1	25	Linear
Meyers	AMMONO	Vertical	450 μm	355	4	9	200	Linear
Meyers	Kyma	Lateral	3 mm	355	0.26	30	100	Linear
Meyers	AMMONO	Lateral	3 mm	355	0.26	37.8	126	Linear
Meyers	Kyma	Lateral	3 mm	355	0.26	33	110	Linear

Table 4: Results from Sullivan, Leach, and Meyers [5] [14] [24]

Based on the work done by Leach, Meyers, and Sullivan, as well as available lab resources, the choice was made to focus primarily on triggering GaN at 532nm. Although there had been no evidence of nonlinear response presented in any of the papers, it appeared to be wavelength that the material was responsive to (demonstrating a low R_{on}) and the lab possessed a testbed operating at 532nm that had been used for lifetime testing in GaAs.

1.6: Purpose of Study

UNM and Sandia have undertaken this project to determine whether GaN possesses a high-gain mode, and if so, what its characteristics are. GaN is a material of interest due to its wide bandgap at 3.44 eV as opposed to the 1.12 eV of Si, 1.43 eV of GaAs, or 3.0-3.3 eV of SiC, allowing for higher power devices in smaller packages.

Conventional GaN devices are becoming more and more common in the power supply industry for this very reason. Combined with the benefits of a PCSS, namely higher switching frequency and less time-domain jitter (in the sub-nanosecond range in GaAs for example) than spark gaps and rise-times in the 100-300ps range, it is an attractive material for the pulsed power community, offering the prospect of a solid-state switch capable of augmenting or replacing spark gap switches in some roles [3] [20]. Unfortunately, all previous efforts in GaN PCSS have operated in the linear regime, meaning that energy transmitted by the switch is directly proportional to the laser energy used to trigger it, rendering it commercially non-viable (a small switch is useless if it requires a laser the size of a lab bench to trigger it). If a high-gain mode can be shown to

exist, this laser energy requirement is obviated, and GaN PCSS may become commercially viable.

The current generation of PCSS are lacking in current carrying capability, voltage hold-off, and/or durability in comparison to spark gap switches, as well as requiring a bulky laser source if the material doesn't possess a high-gain mode. If GaN can be shown to exceed SiC and/or GaAs in any of these categories, it may be a viable alternative to spark-gap switches in some applications. A smaller, more reliable, high power solid state switch is of tremendous interest to the pulsed power community due to the improvement in shot to shot repeatability and reliability relative to current switch designs. Additionally, the ability to operate the switch at multiple kHz, or even MHz offers a tremendous advantage over spark gap switches, which are limited to hundreds of Hz in most cases [25].

As no previous effort has shown evidence for a high-gain mode in GaN, this work will be the first in-depth verification of the existence of and characterization of a high-gain mode in GaN and will help guide the next generation of research and development in this material and mode. [1] [14] [24].

Chapter 2: Devices and Methods

2.1: The Devices

2.1.1: Introduction

Lateral PCSS devices are not widely commercially available, and those which are, are packaged in a way that makes them unsuitable for the experimentation the author wished to perform. Thus, it was necessary for Sandia National Laboratories to produce their own devices "in-house". Two different vendors (Kyma Technologies and AMMONO) were chosen to supply bulk GaN, as they used different processes and dopants, which could potentially impact the experimental results. Once the bulk GaN was received, it was processed and made into devices by the Semiconductor Material & Device Sciences group at Sandia National Laboratories. Three usable device lots were created in total, Kyma Lot 1, Kyma Lot 3, and AMMONO Lot 1. Kyma Lot 2 was unsuitable for use and scrapped.

2.1.2: Device Fabrication

Each sample was prepared by attaching planar electrodes onto a GaN substrate using standard photolithography, electron-beam metal evaporation, and metal-liftoff techniques. The contact, consisting of a Ti/Al/Ni/Au metal stack, was then annealed at 800 C for 1 min in a rapid-thermal annealing system to promote adhesion of the contact metals. Using similar techniques, a Ti/Au bond pad, for electrical probing and package wire-bonding was formed on the original contact metals. Finally, the devices were singulated into die using a dicing saw for packaging and device characterization.

2.1.3: Device Geometry

After singulation, it was determined that only the 600 μm gap (distance between pads) devices were useable due to breakage during the dicing process. Thus, all devices used for this thesis possessed the lateral geometry shown in Figure 8.

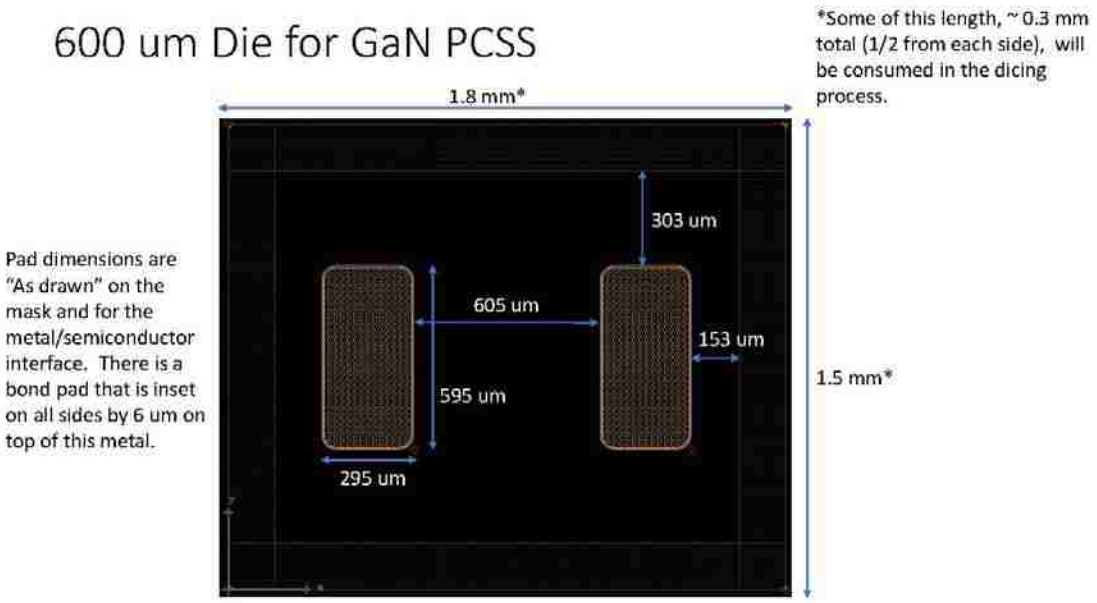

Figure 8: Nominal Device Geometry

The AMMONO GaN devices were slightly thinner than the Kyma GaN devices, measuring 380-385 μm thick as opposed to the 595 μm thickness of the Kyma.

2.1.4: Device Characterization

Before testing any new device, it is essential to determine some of its electrical characteristics. For switches, two critically important parameters are hold-off voltage and off-state resistivity (along with on-state resistivity, but this is determined during device testing). Hold-off voltage refers to the maximum voltage the device can withstand before it self-triggers and conducts electricity. Off-state resistivity refers to the resistance a

device has when it is in an "off" or non-conductive state. In an ideal switch, the hold-off voltage and off-state resistivity are both infinite, i.e., no unwanted flashover occurs through or across the switch, and no current leaks through it.

After fabrication but before dicing, flashover testing was performed. Flashover testing is used to determine what the device hold-off voltage is. By determining this voltage, it is then possible to operate the device up to this limit and avoid randomized and potentially hazardous or damaging electrical discharges that can occur if the voltage across the device is higher than what it can hold-off. Additionally, it can inform the effectiveness and/or need for a dielectric passivation layer on the surface of the device. Passivation layers are used to electrically insulate the surface of a device, reducing the chance of surface flashover through air as well as protect it during handling and use.

Flashover testing showed that hold-off field strength was inversely proportional to the gap size of the device, which is to be expected given that it is proportional to $1/\sqrt{L}$, where L is the length of the gap [26]. When flashover testing was also performed with a passivating silicon nitride layer atop the device, it did not impact the results. Because there was no benefit to the silicon nitride layer it was decided to not use a passivation layer on future device lots to simplify and reduce the cost of fabrication.

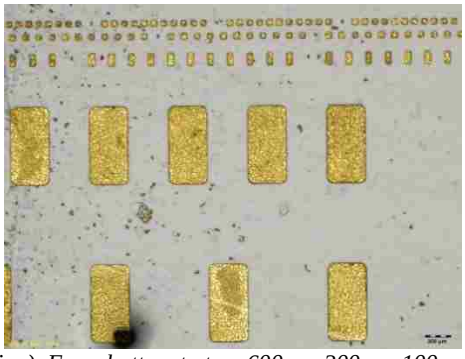

Figure 9: Kyma Lot 1 (pre-dicing). From bottom to top, 600um, 300um, 100um, 50um, and 25um pad spacing

Substrate	Gap (μm)	Flashover (kV)	Medium	Pulse Width (ns)	kV/cm
GaN	600	1.7	air	500	28
	600	1.8	air	500	30
	600	2.5	air	500	42
	300	1.5	air	500	50
	300	1.6	air	500	53
	100	1.2	air	500	120

Table 5: Gap size vs. Flashover Voltage

2.1.5: Device I-V Curves

To characterize the off-state resistances of the devices, samples of all 3 lots were characterized by a Keysight B1505A curve tracer under Fluorinert FC-70 dielectric fluid. The curve tracer is a device used to monitor the current through a device as a function of voltage in the time domain. When the device is off, this current is known as the “dark current” or “leakage current” and combined with the voltage across the device can be used to calculate the off-state resistivity. The Fluorinert FC-70 functioned as an insulating dielectric to prevent arcing and flashover during testing, as it has a much higher breakdown strength than air (157kV/cm vs 30kV/cm).

This produced the following representative results. As can be seen in Figure 10 and Figure 11 the leakage current for the AMMONO GaN is in the 10s of picoamperes range, whereas that for the Kyma GaN is in the microamperes. The AMMONO devices routinely held off more than 8kV (133 kV/cm). Based on these charts, the resistivity of the AMMONO GaN used is greater than 333 TΩ/cm, 4 orders of magnitude higher than that of the Kyma GaN.

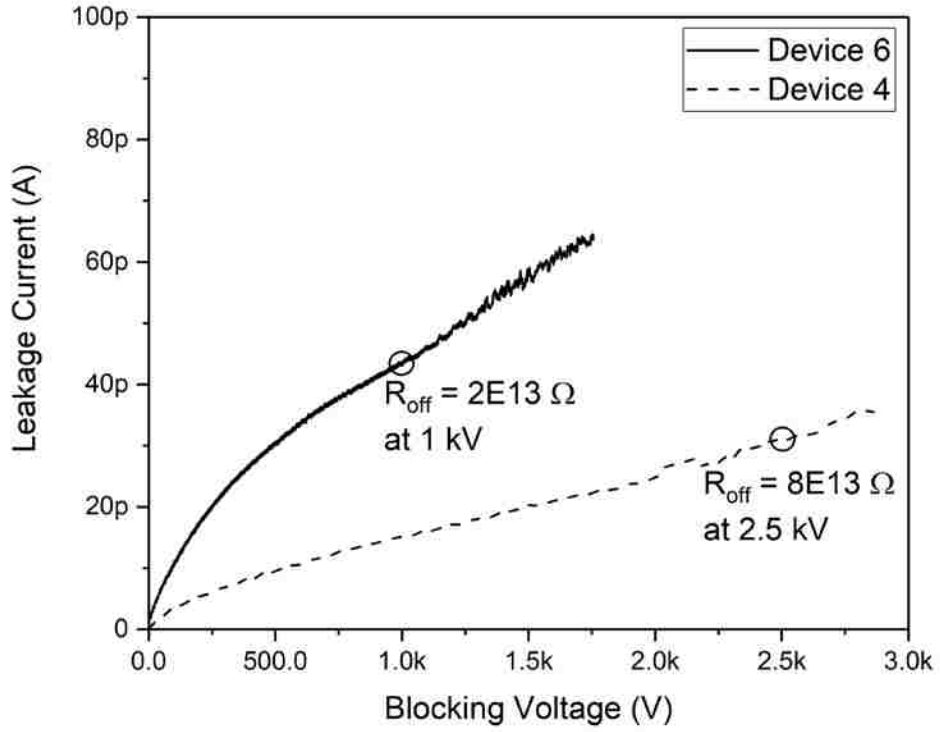

Figure 10: AMMONO Representative Leakage Current (pA)

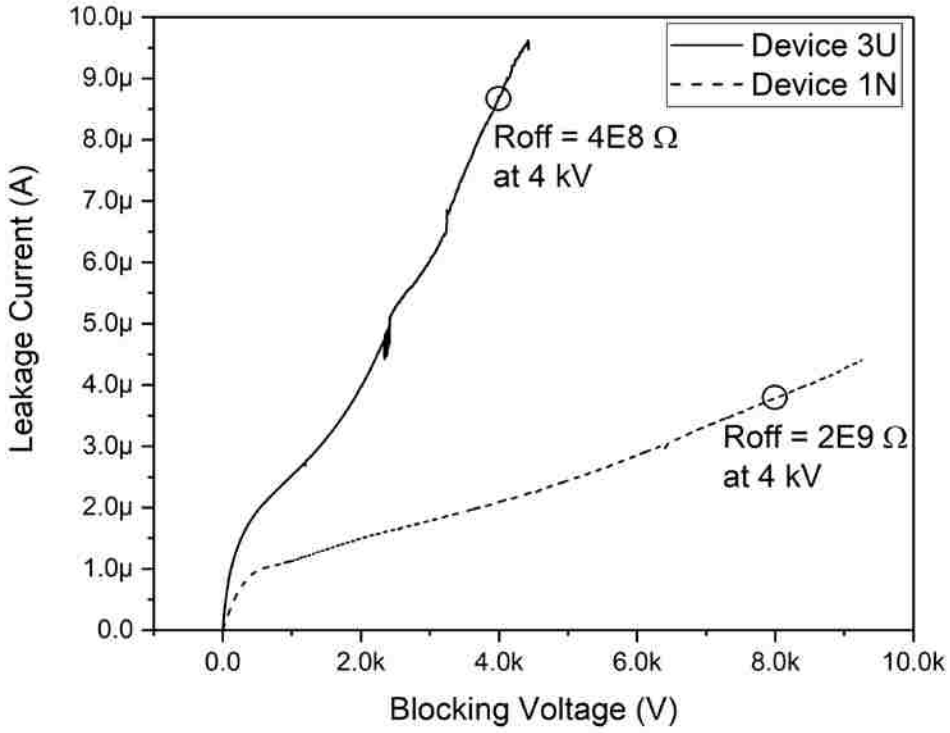

Figure 11: Kyma Representative Leakage Current

2.2: Instrumentation

Below is a list of the measuring devices used to monitor and log experimental results throughout this thesis. All equipment was calibrated in accordance with Sandia National Labs policy and NIST standards.

Oscilloscope – Tektronix DPO 5205B, 2GHz, 10Gs/s

CVR – T&M SSDN-10TT

Camera – Allied Vision Technologies Manta G-283B

2.3: Test Setup

Given the results of the literature review, as well as a lack of responsivity doing some preliminary testing at 800nm, the decision was made to switch to the use of an existing testbed in the lab. This setup had been extensively used for lifetime testing in GaAs PCSS devices, and was well characterized and understood by the lab technicians and program manager. One of the key features of this testbed was the ability to image the device to confirm the presence or lack thereof of filamentation during device operation.

The test setup consisted of a Bertan Series 105-10R power supply feeding into a FR4 board with a copper center conductor and ground rails. On some tests, a 1500pF input capacitor was used to supply higher currents during switching operations. The test sequences using this capacitor will be clearly marked. The two input configurations can be seen in Figure 12.

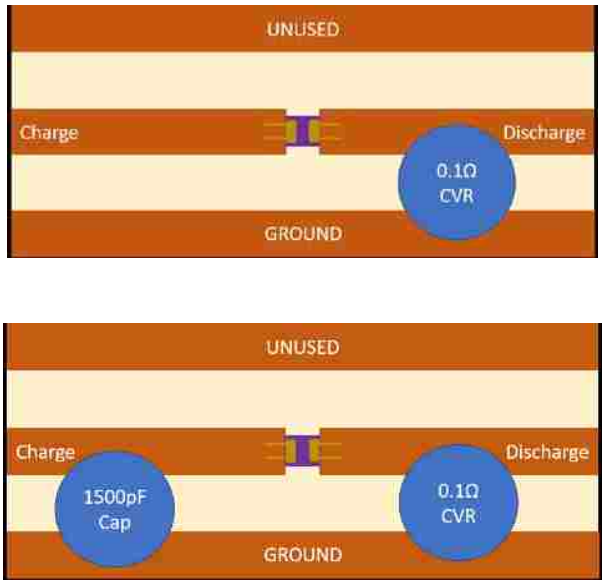

Figure 12: PCSS Board without (top) and with (bottom) input capacitor

A small (~1mm) gap was incised in the center conductor, and the GaN device was secured in the gap by means of a cyanoacrylate adhesive (superglue). Gold ribbon (25x100 μm) was then used to bond the device to the conductor, with two wire bonds each on the anode and cathode, as in Figure 13.

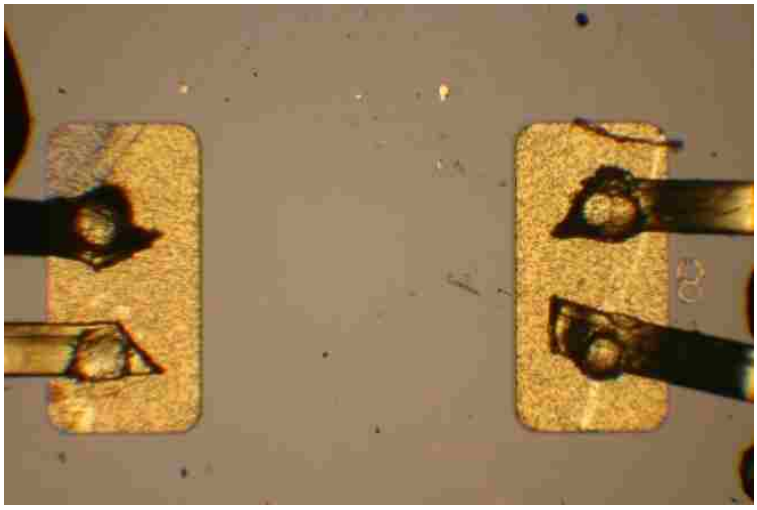

Figure 13:Example of wirebonds on PCSS

On the discharge side, a 0.1 Ω current viewing resistor (CVR) was placed to monitor the current flowing through the device.

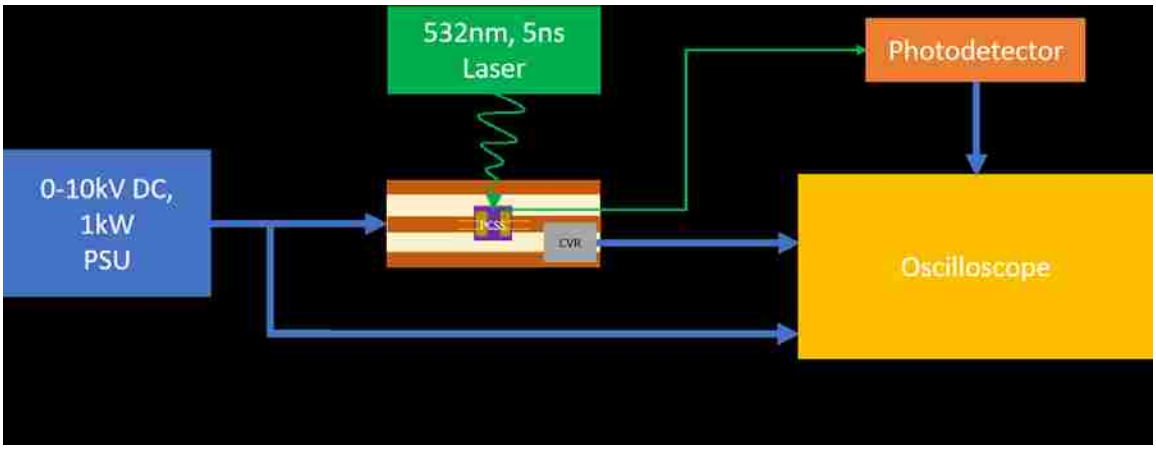

Figure 14: Test Setup Block Diagram

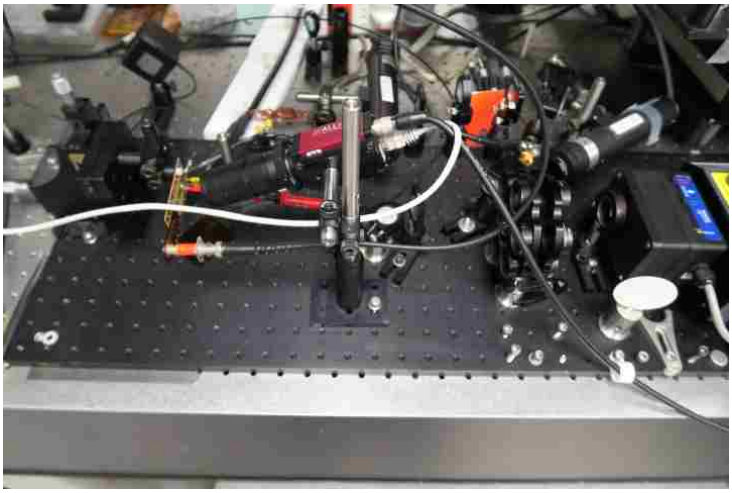

Figure 15: Test Setup Image

Initial attempts to trigger the device were made at 800nm, but only produced a very small linear response as the photon energy was too far below bandgap. Based on [14], the decision was made to instead test at 532nm with a 5ns pulse width using a New Wave Polaris II ND: YAG laser, frequency doubled from 1064nm to 532nm. Laser power was measured using a portable laser power meter and output power was varied by inserting optical filters of appropriate density.

A Tektronix TEK P6105 oscilloscope probe (10x, 100MHz, 1MΩ, 13pf input capacitance) was used to monitor the charge voltage, and a BNC connector was used to monitor the voltage across the current viewing resistor. A photodetector was used to monitor the laser pulse and determine timing relative to the output waveform. Below is an example of the timing used for this circuit, showing that at the time of triggering, the charge voltage is in a steady-state condition. All probes/detectors were used with a Tektronix DPO 5205B oscilloscope. An Allied Vision Technologies Manta G-283B camera was also configured to image the device to capture any potential filaments. This camera uses a GigE interface and has configurable gain and exposure, which helps with imagery timing and optimization.

Figure 16: Test Setup Timing

Chapter 3:

3.1: Kyma Lot 1

Using the above test setup, the first round of testing was done with the Kyma Lot 1 device in Figure 17. The image shows substantial metallization between the contacts, which was due to the immaturity of the process used to create these devices.

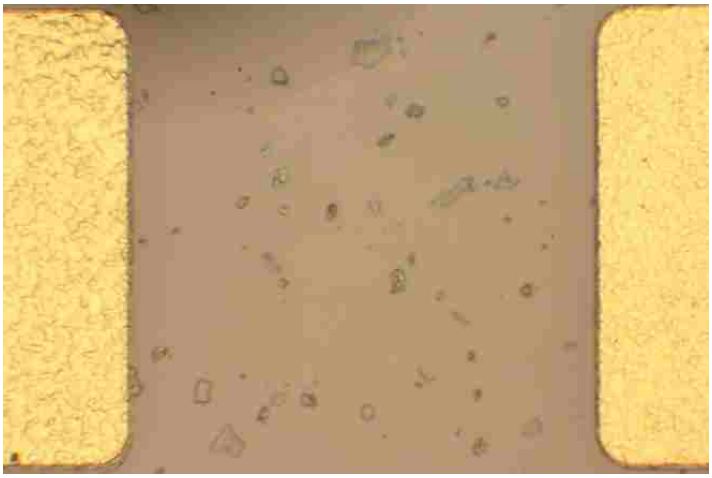

Figure 17: Kyma Lot 1 Device

Testing started by applying a 0V bias and impacting the device with nominally 8mJ of laser energy. The photoelectric effect (the emission of electrons by a material in response to incident photons) produced 7mA of current in response, which indicated that the GaN used for this testing was responsive at 532nm, in contrast to the efforts made previously at 800nm by our team. This also validated the results and methodology used by Leach [14].

It was assumed that if GaN had a high-gain mode, that it would manifest similarly to the persistent optically induced conductivity seen in other group III-V semiconductors, such as GaAs, demonstrating a linear response concurrent with the laser, followed by a nonlinear persistent conductivity shortly after. The delay between linear and nonlinear

response would be influenced both by the voltage field strength across the device as well as the optical energy used to trigger it.

Figure 18: Kyma Lot 1 Photoelectric Effect

The voltage was then raised to a nominal 1000V (976V measured), which translates to a field strength of 16.27kv/cm. The device was triggered with 2 mJ of laser energy and produced a noisy, but distinctly nonlinear phenomenon as well as a very small filament on the device, as can be seen in Figure 20 and Figure 21. The filament was captured using an Allied Vision Technologies Manta camera. The camera was triggered

by the emission of the laser pulse, and exposure and gain settings were manually configured to capture an image of the device immediately following that signal.

The current peak of 17.2A shown in Figure 20 was measured across a current viewing resistor. The charge voltage was measured across the output of the power supply, as shown in the circuit of Figure 19

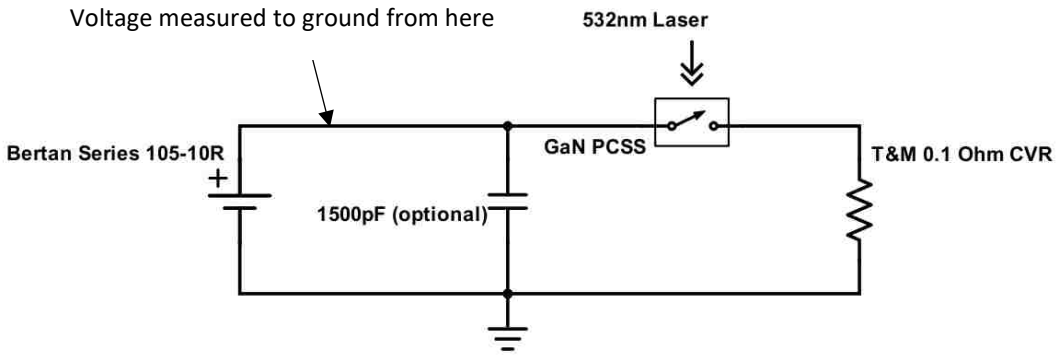

Figure 19: Test Circuit Schematic

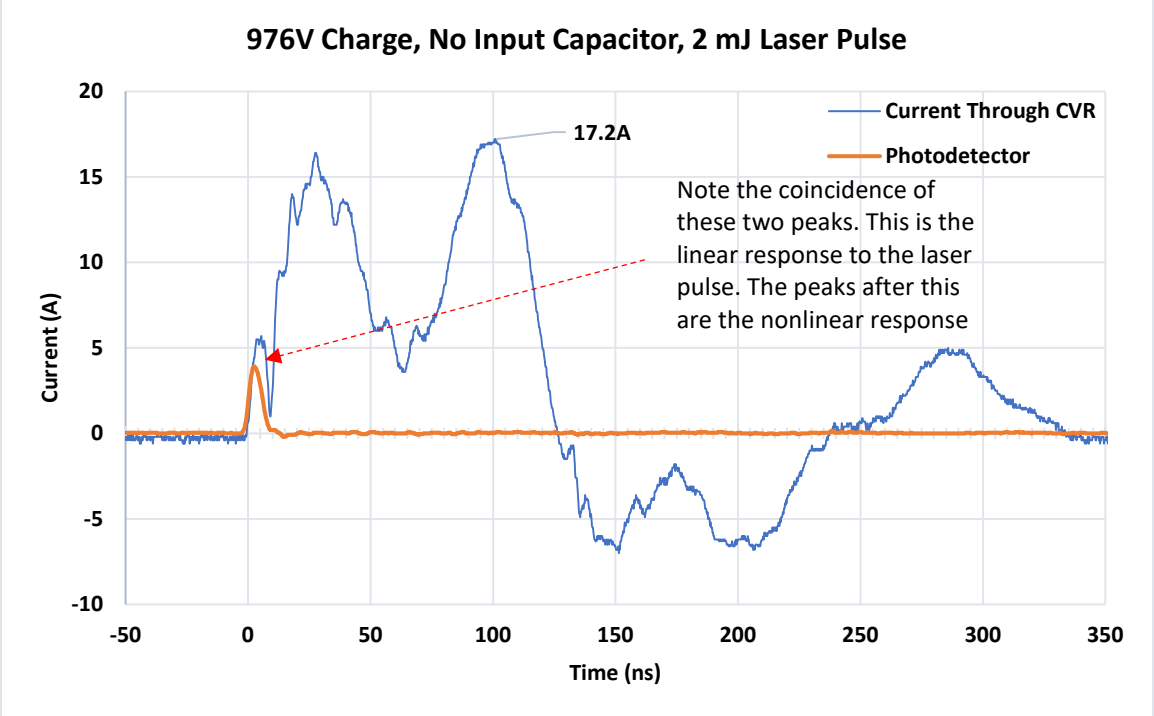

Figure 20: Kyma Lot 1 Nonlinear at 976V, 2mJ laser pulse

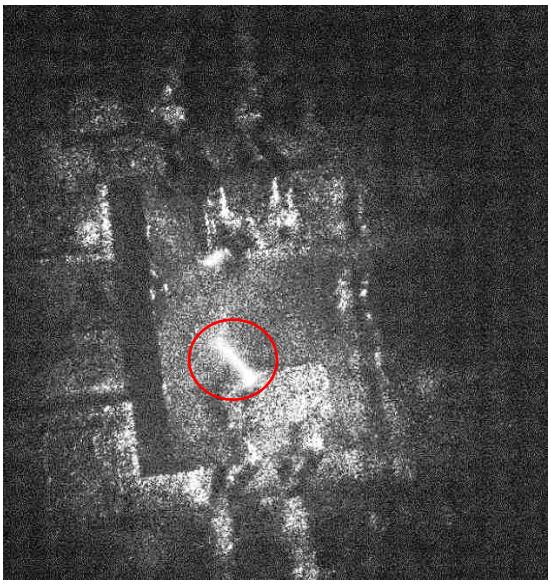

Figure 21: Kyma Lot 1 filament at 976V, 2mJ laser pulse. Filament circled in red

The above was the first evidence for nonlinear behavior in GaN, but the measured current was relatively low and the device itself was not well finished, as it was from the first batch of devices. To provide more electrical energy on the charge side, as well as reduce the noise on the signal, a 1500pF capacitor as in Figure 12 (bottom) was added to the device. This provided an energy storage device to source more current than the power supply could provide, as well as functioning as a capacitive filter. Because 1000V (nominal) was arbitrarily chosen, it was then necessary to reduce the charge voltage to a point where the device operated in the linear mode, then increase it until the threshold between linear and nonlinear behavior was determined.

Voltage across the device was increased incrementally starting from 400V until nonlinear behavior was observed. The decision was made to remain at 2mJ of laser energy per shot to reduce the number of variables, as the voltage threshold for nonlinear behavior varies with laser trigger energy. In general, the lower the laser trigger energy, the higher the voltage on a given device needs to be. An example of the linear behavior

for this device at 484V is shown in Figure 22. Please note that the photodiode was uncalibrated and was used for triggering and timing purposes rather than measurement of laser output power. It also served to clearly illustrate that the linear response of the GaN PCSS is directly related to the laser pulse, as the pulse widths are almost identical.

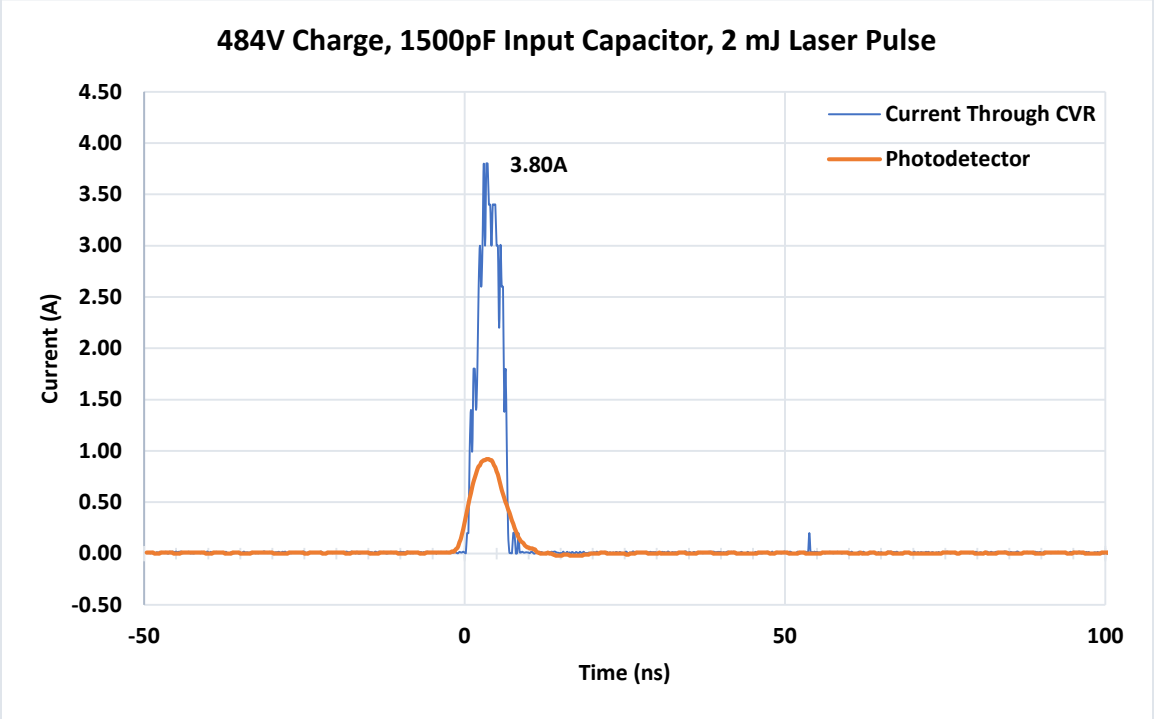

Figure 22: Kyma Lot 1 Linear at 484V, 2mJ laser pulse, 1500pF input capacitor

At 512V, a delayed nonlinear response was seen, ~50ns after the linear switching from the laser (Figure 23) and a filament was formed (Figure 24). There was also a secondary peak of unknown origin.

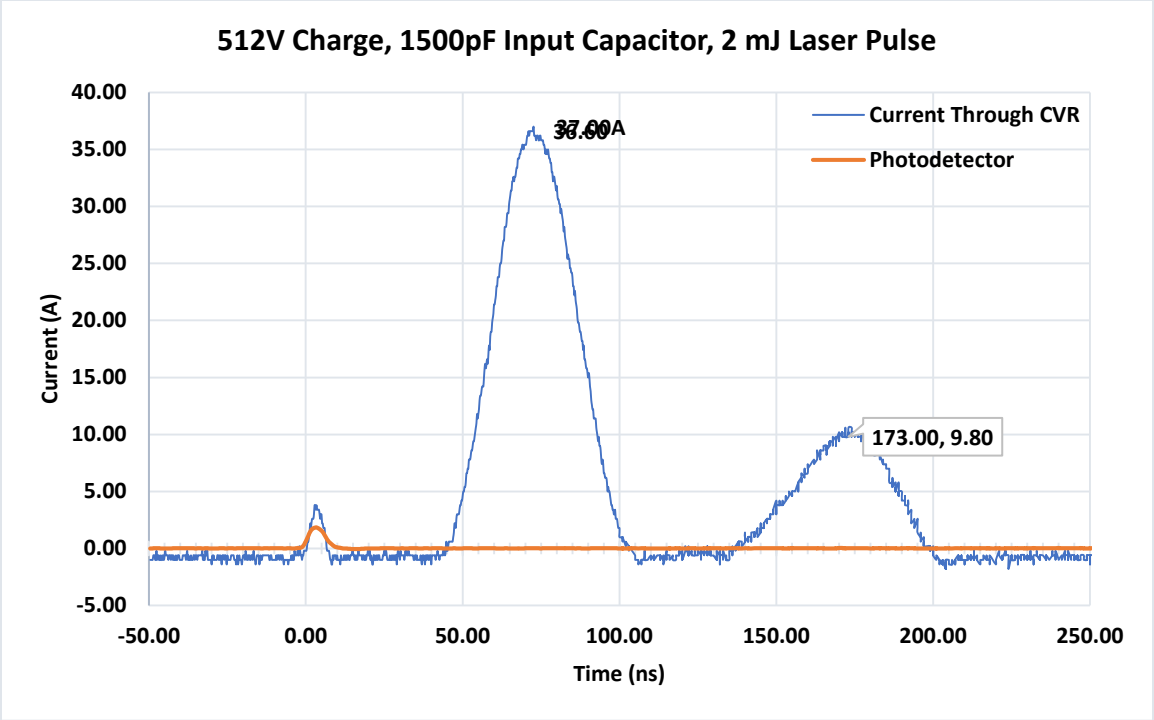

Figure 23: Kyma Lot 1 Nonlinear at 512V, 2mJ laser pulse, 1500pF input capacitor

Figure 24: Kyma Lot 1 filament at 512V, 2mJ laser pulse, 1500pF input capacitor

Voltage was then increased further, to 734V, and the same nonlinear phenomenon was observed. Additionally, increasing the voltage drove the nonlinear behavior to earlier development, as can be seen in Figure 25.

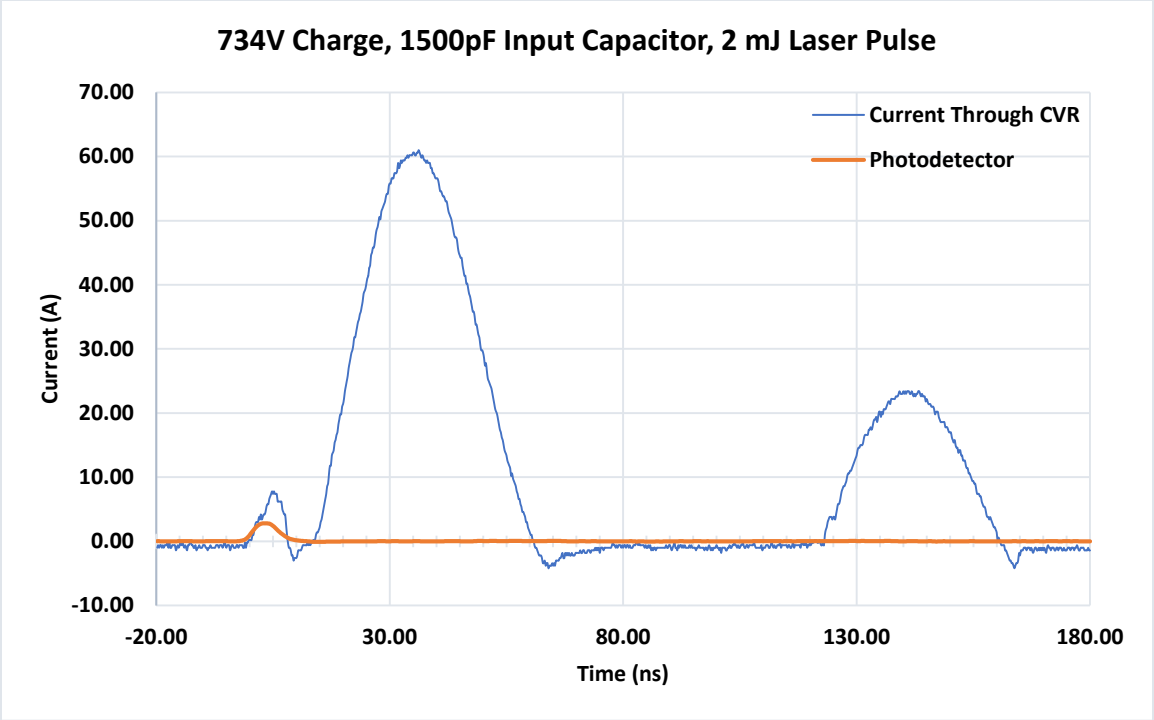

Figure 25: Kyma Lot 1 Nonlinear at 734V, 2mJ laser pulse, 1500pF input capacitor

Figure 26: Kyma Lot 1 filament at 734V, 2mJ laser pulse, 1500pF input capacitor

The above results provided evidence of a nonlinear phenomenon occurring, but questions remained as to the validity of the results due to the following factors.

- The surface of the device was not well-finished.
- Filamentation was not visible across the entire gap.
- The device failed catastrophically (Figure 27).

- Impact of the metallization within the gap on filament formation?
- Was the observed phenomenon a high-gain mode or surface flashover?

However, the initial results were intriguing enough to justify testing Kyma Lot 3 which was of much higher quality and would answer some of these questions and concerns.

Figure 27: Kyma Lot 1 Device Failure

3.2: Kyma Lot 3

The same testbed and circuit set-up used for Kyma Lot 1 was used for the Lot 3 device, but it was theorized that if the surface metallization between the contacts was indeed reducing the effective gap width, higher voltages and more laser energy would be needed to make the device behave in a nonlinear fashion. Thus, the decision was made to use a higher laser trigger energy than was used for Kyma Lot 1. Figure 28 shows that apart from a non-metallic smear on the surface, the Lot 3 device is clean.

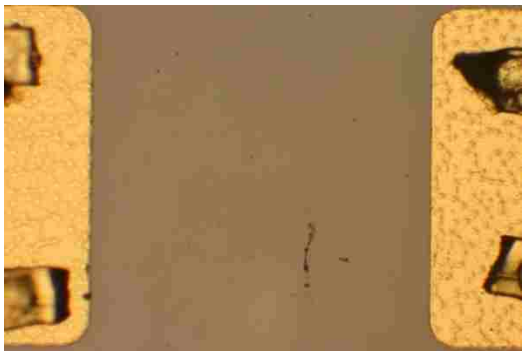

Figure 28: Kyma Lot 3 Device

Testing started at 179V (200V nominal), which equates to 3.33kV/cm field strength, using 12.5mJ of laser energy, and produced linear results. Voltage was increased in 100V increments, resulting in waveforms like the following in Figure 29.

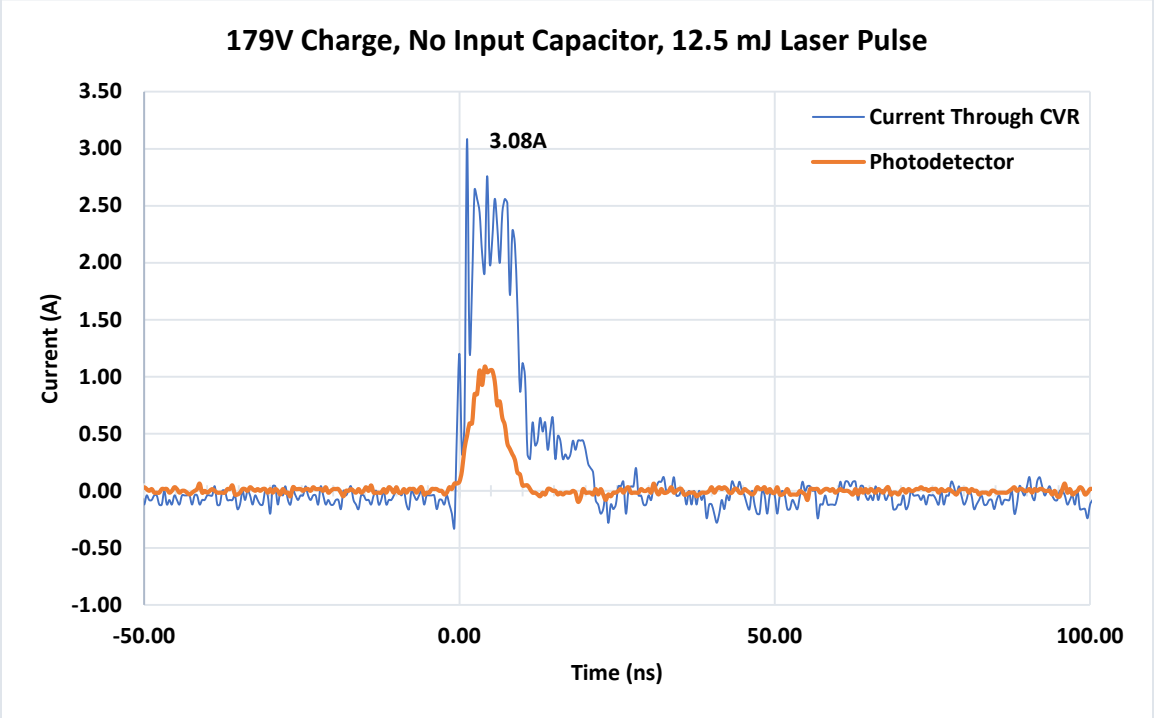

Figure 29: Kyma Lot 3 Linear at 179V, 12.5mJ laser pulse

At 700V nominal (647V measured) a nonlinear result was observed, so voltage was reduced incrementally until triggering was unreliable; with some shots exhibiting linear behavior and others exhibiting nonlinear behavior. An example of the nonlinear

behavior near this threshold is shown in Figure 30. Like Kyma Lot 1, a substantial (~75ns) delay between linear and nonlinear response near the threshold can be seen.

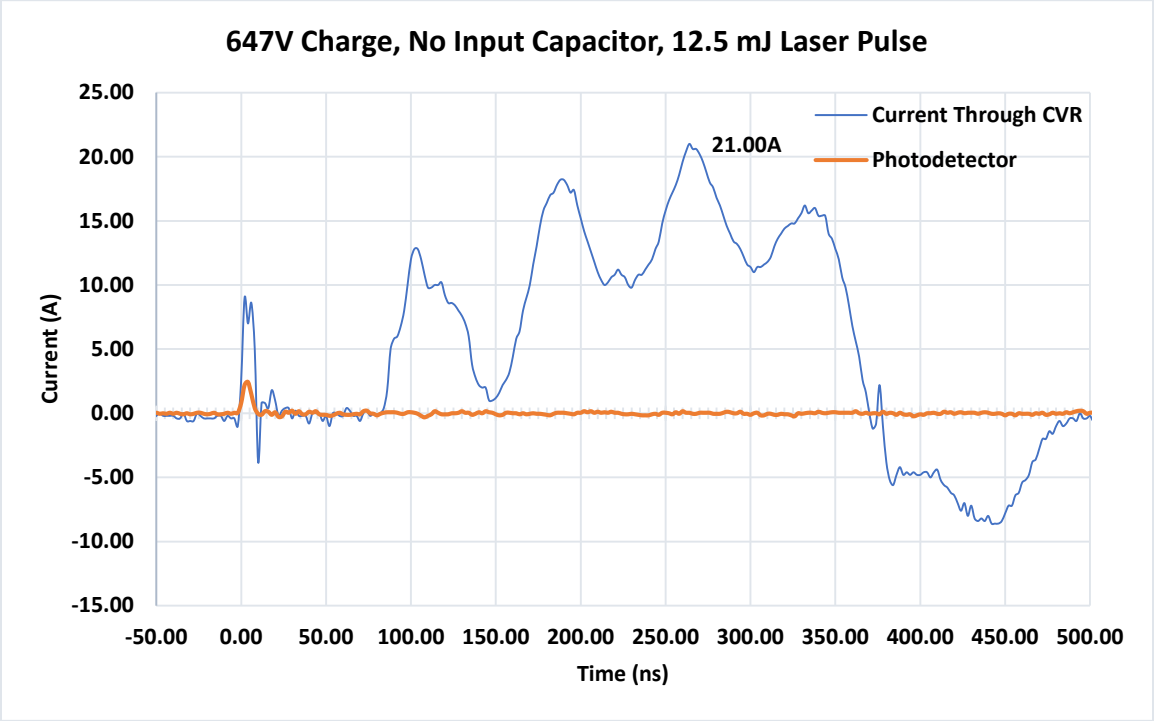

Figure 30: Kyma Lot 3 Nonlinear at 647V, 12.5mJ laser pulse

The 1500pF capacitor was then added to the input and testing resumed; restarting at 200V and increasing until nonlinear behavior was reliably triggered, around 700V nominal (Figure 31 and Figure 32). Filamentation characteristic of high-gain operation (such as that seen in GaAs) was again captured by the camera, further supporting the results from Lot 1.

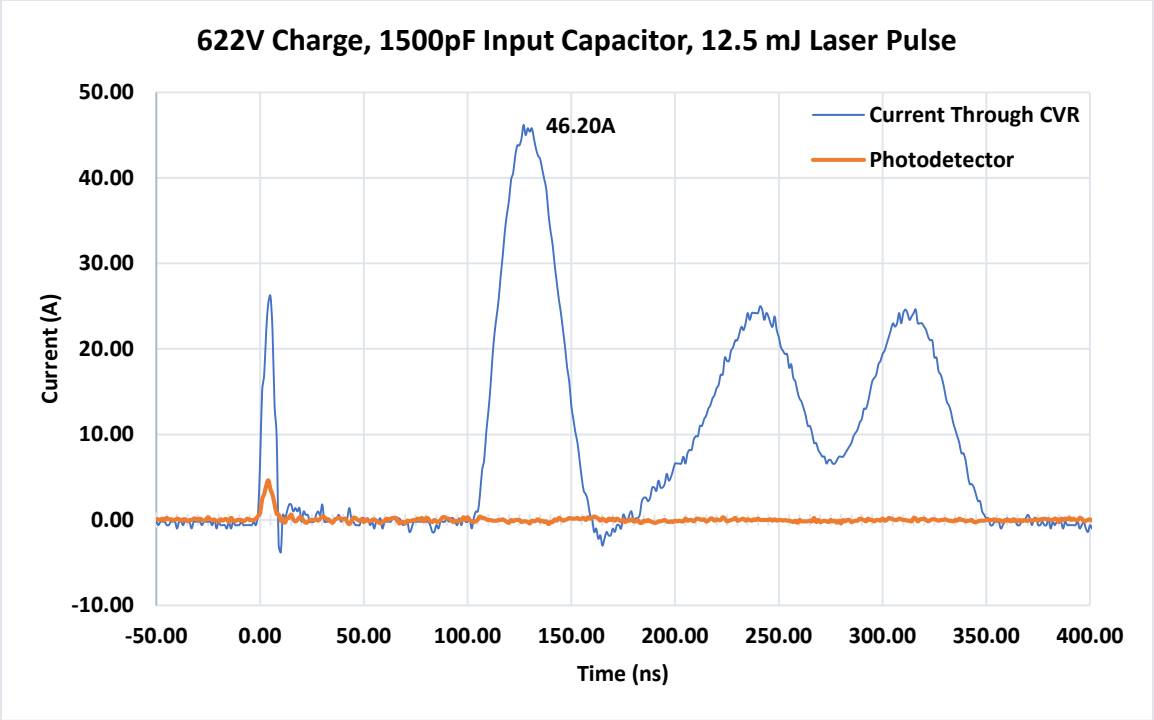

Figure 31: Kyma Lot 3 Nonlinear at 622V, 12.5mJ laser pulse, 1500pF input capacitor

Figure 32: Kyma Lot 3 filament at 622V, 12.5mJ laser pulse, 1500pF input capacitor

As it had been proven that that this nonlinear phenomenon was real and not an artifact of the poorly processed device from Lot 1 or experimental error, a decision was then made to test the relation between field strength (volt/cm), and laser energy (mJ). Table 6 contains the findings. From these results, a rough "rule of thumb" was derived for future testing. For every 30V (500V/cm) increase in supply voltage, laser energy could be reduced by 1 mJ.

Nominal Voltage	Field Strength (kV/cm)	Required Laser Energy for Nonlinear Response (mJ)
700V	11.67	12.5
800V	13.33	7
850V	14.17	5
950V	15.83	4

Table 6: Voltage vs Laser Energy for Nonlinear Mode

One of the remaining concerns was the unusual delay between linear and nonlinear switching. Based on the team's previous experiences working with GaAs PCSS, the decision was made to increase voltage across the device while using a high laser input energy of 12.5mJ. Testing started at 1199V, 12.5mJ, and immediately reduced the time-domain separation of the linear and nonlinear modes (Figure 33). To avoid overloading the scope, output of the CVR was passed through a 2x attenuator. This resulted in 107A at 1199V for a shot power of 128kW. Voltage was then increased in 100V increments, ending in a final shot at 1456V, 97A through 5x attenuation, resulting in a peak shot power greater than 141kW (Figure 34).

A comparison between Figure 31 and Figure 33 shows that increasing field strength reduces the gain between linear and nonlinear mode and starts to force an overlap of the two modes, as expected by the team. Voltage was increased until a surface flashover was

triggered several times (nominally 1700V), then reduced to 1500V and the device was operated in both linear and nonlinear modes for several more shots without failure.

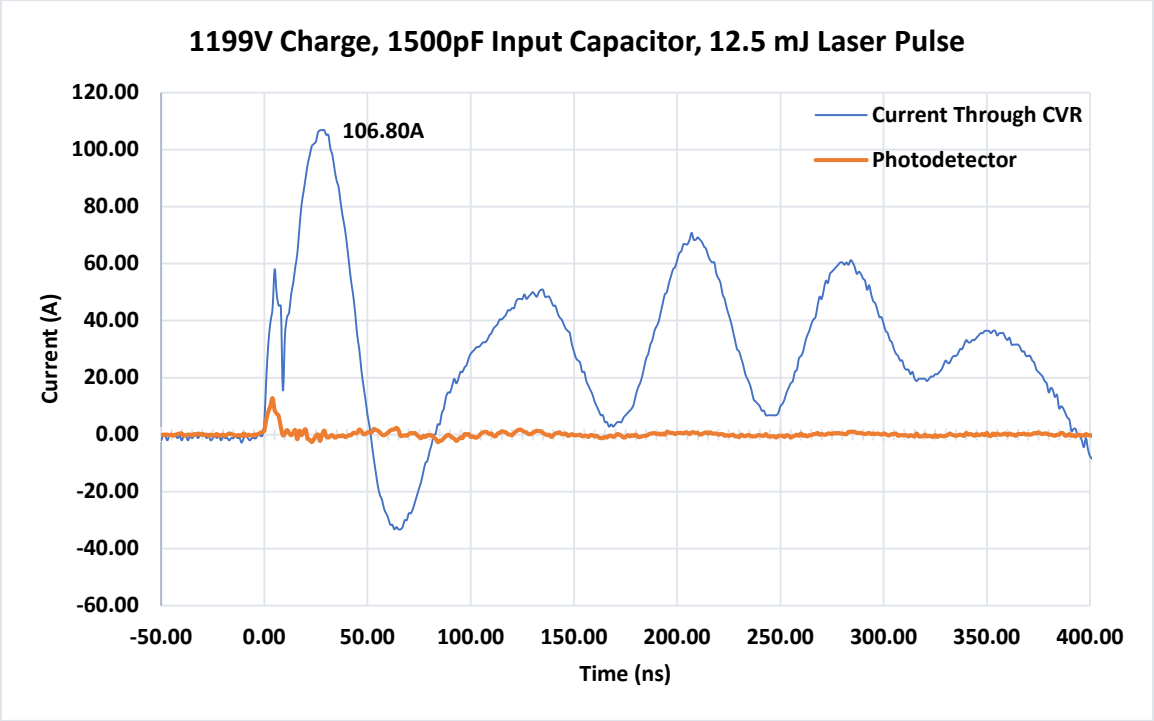

Figure 33: Kyma Lot 3 Nonlinear at 1199V, 12.5mJ laser pulse, 1500pF input capacitor, 2x attenuator

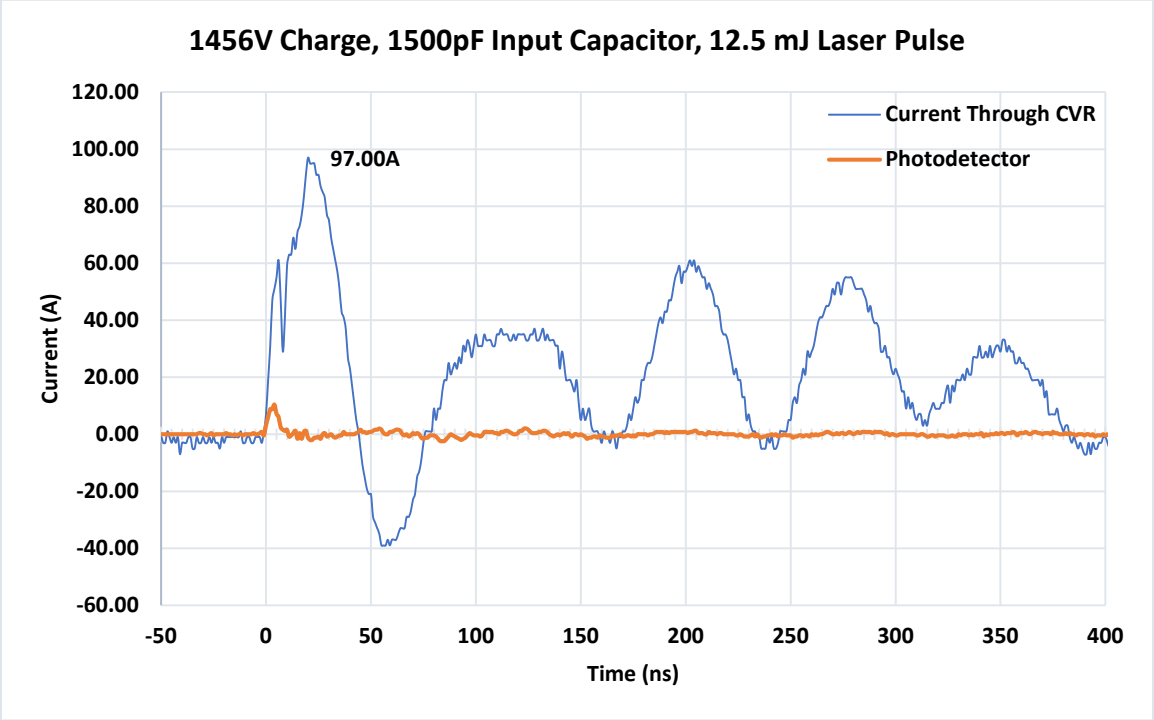

Figure 34: Kyma Lot 3 Nonlinear at 1456V, 12.5mJ laser pulse, 1500pF input capacitor, 5x attenuator

Lot 3 had far better durability than Lot 1, but still suffered from degradation of the electrodes throughout testing as can be seen below. Additionally, an odd “rainbow” discoloration was formed on the discharge side (Figure 35). Given these results, it may be prudent to revisit the electrode geometries on the next batch of devices.

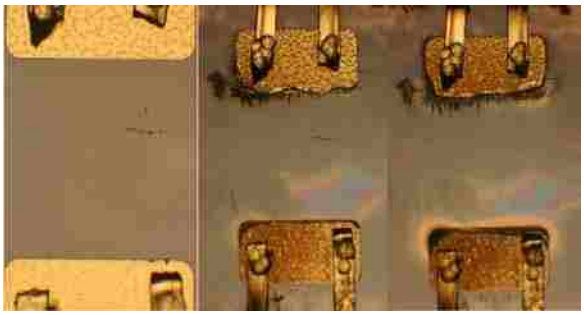

Figure 35: Kyma Lot 3 Device after use

Lot 3 validated the results from Lot 1 and removed any questions about the impact of metallization on the nonlinear phenomena. A repeatable, high-gain nonlinear response was seen at 532nm (below bandgap energy), at laser pulse energies as low as 4mJ. The occurrence of this high-gain mode while using a sub-bandgap trigger alleviates potential issues with current crowding as well as surface flashover, as it allows for the utilization of the bulk of the material for current transport, rather than the surface of the device. This phenomenon was tested to field strengths of 24.3 kV/cm, and at a variety of voltages and laser pulse energies.

After examining the charge waveform and comparing it to the output across the CVR, it appeared that many of the secondary peaks were related to the power supply attempting to “recharge” and get back to the bias voltage, as shown in Figure 36. In future, it is recommended that a zero-clamped power supply be used to prevent this behavior.

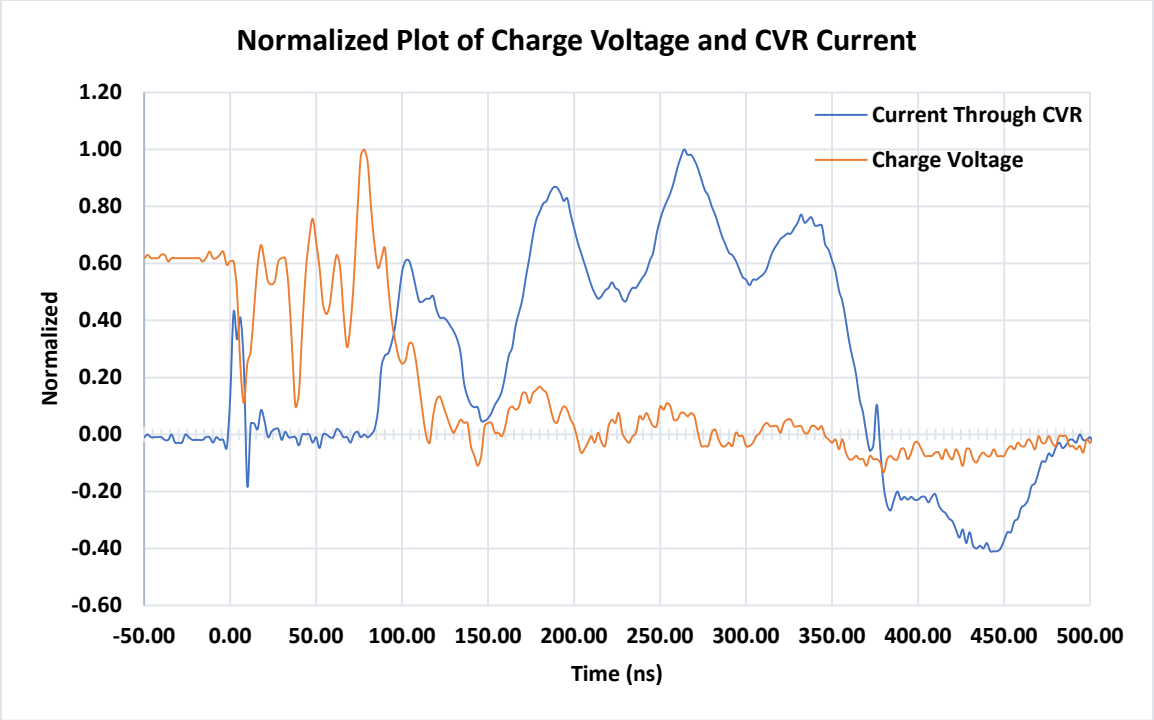

Figure 36: Charge Voltage and CVR Voltage. Note the coincidence of peaks of the CVR with zero crossings of the charge voltage.

The next step was to examine whether this nonlinear mode was exclusive to Kyma GaN, or whether it existed in material from other manufacturers as well.

3.3: AMMONO GaN

The other source of GaN for this project was AMMONO. The AMMONO GaN differs from the Kyma GaN in that it has far higher off-state resistivity, as well as using a different dopant, leading to a deep orange color to the naked eye. Based on discussions with the lab that created the devices, it appears that the Kyma GaN is unintentionally Fe doped, whereas the AMMONO GaN is Mg doped. Figure 37 shows that the AMMONO GaN is relatively well finished, being almost entirely free of metallization between the contacts. The devices were inconsistent in finish quality due to the immaturity of the process used to create them. Kyma Lot 1 was the first batch of GaN PCSS produced by the fabrication group (thus explaining the comparatively poorer finish), Kyma Lot 2 was

lost during fabrication, and both the AMMONO and Kyma Lot 3 were produced immediately following that. Both Kyma Lot 3 and AMMONO leveraged the lessons learned from Kyma Lots 1 and 2 for a superior product.

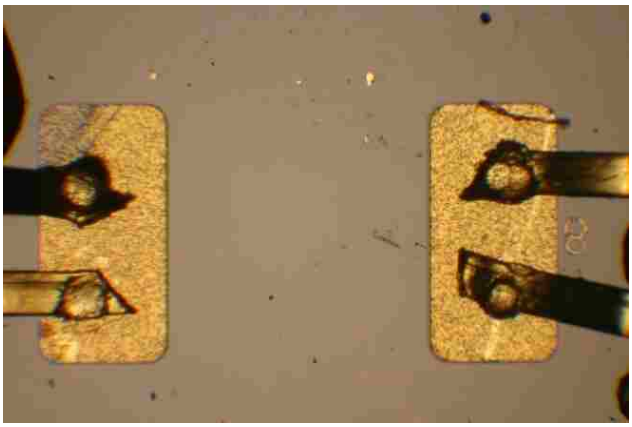

Figure 37: AMMONO GaN Device

The same testbed and test circuit was used for AMMONO GaN as for Kyma Lots 1 and 3 to reduce variability in results. The test circuit used no input capacitor and a starting voltage of 200V nominal. Voltage was then increased in 100V increments until a nonlinear response was observed. Doing so allowed the AMMONO device to be compared directly to the Kyma devices.

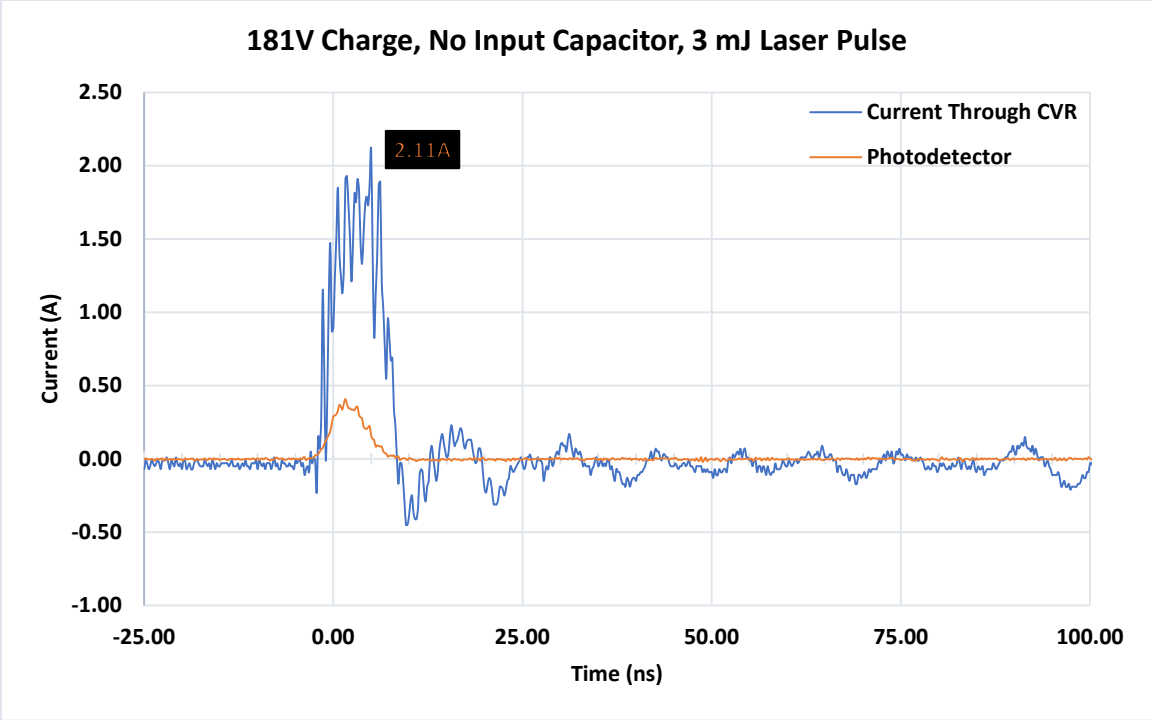

Figure 38: AMMONO GaN Linear at 181V, 3mJ laser pulse

It was immediately evident that the AMMONO GaN was more responsive at lower laser energy levels than the Kyma GaN. Figure 38 shows that in the linear mode, the AMMONO GaN conducted more than twice the current with less than a quarter of the laser trigger energy compared to Kyma Lot 3 (2.11A at 3 mJ vs 3.1A at 12 mJ). Repeatable triggering of the nonlinear mode was observed around 880V, which is much higher than the threshold voltage observed in Kyma Lot 3. This result is to be expected given the reduced laser energy and the previously explored inverse relationship between field strength and laser energy. Figure 39 and Figure 40 show an example of the nonlinear mode, as well as filaments from 6 separate shots. These filaments could be moved around the device by moving the location of the laser beam. This observation is significant, as it further indicates that the filaments are optically triggered, and not a result of surface flashover. As previously noted, this close to threshold there was about a 100ns delay between linear and nonlinear modes.

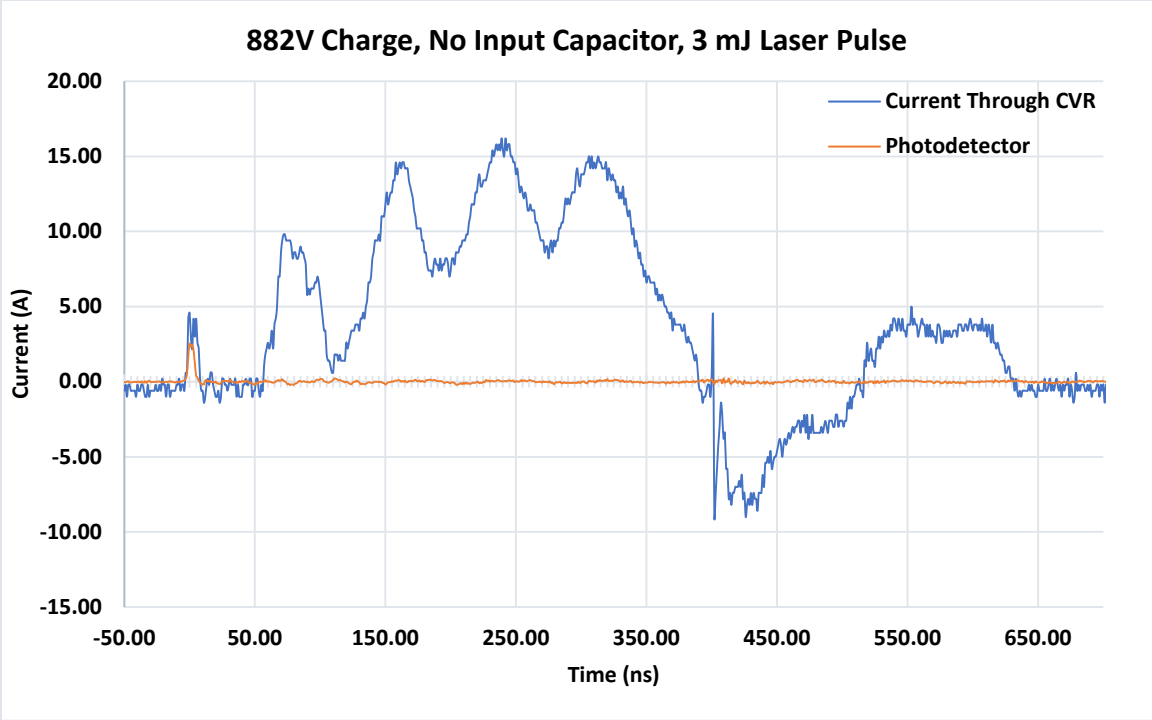

Figure 39: AMMONO GaN Nonlinear at 883V, 3mJ laser pulse

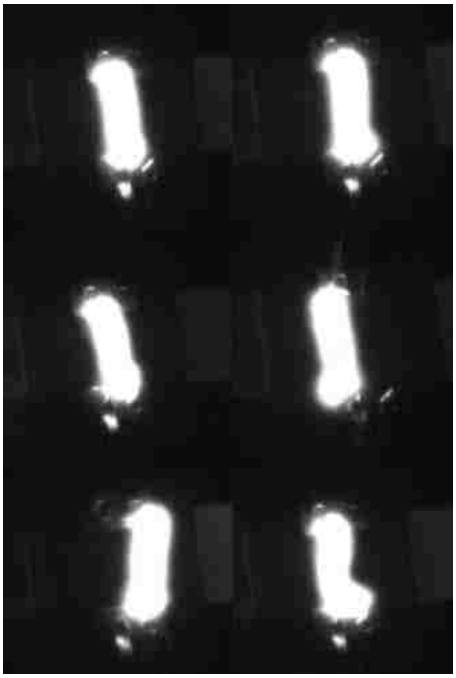

Figure 40: AMMONO GaN filaments at 883V, 3mJ laser pulse

The previously derived relation between field strength and laser pulse energy from Table 6 was then tested. Given it was possible to trigger at 950V with 3mJ, it was theorized that above 1050V less than 1mJ of energy would be needed to trigger the device. This hypothesis was proven correct when a nonlinear response was triggered at 1088V with only 300μJ of laser energy, yielding 19.8A in the nonlinear mode.

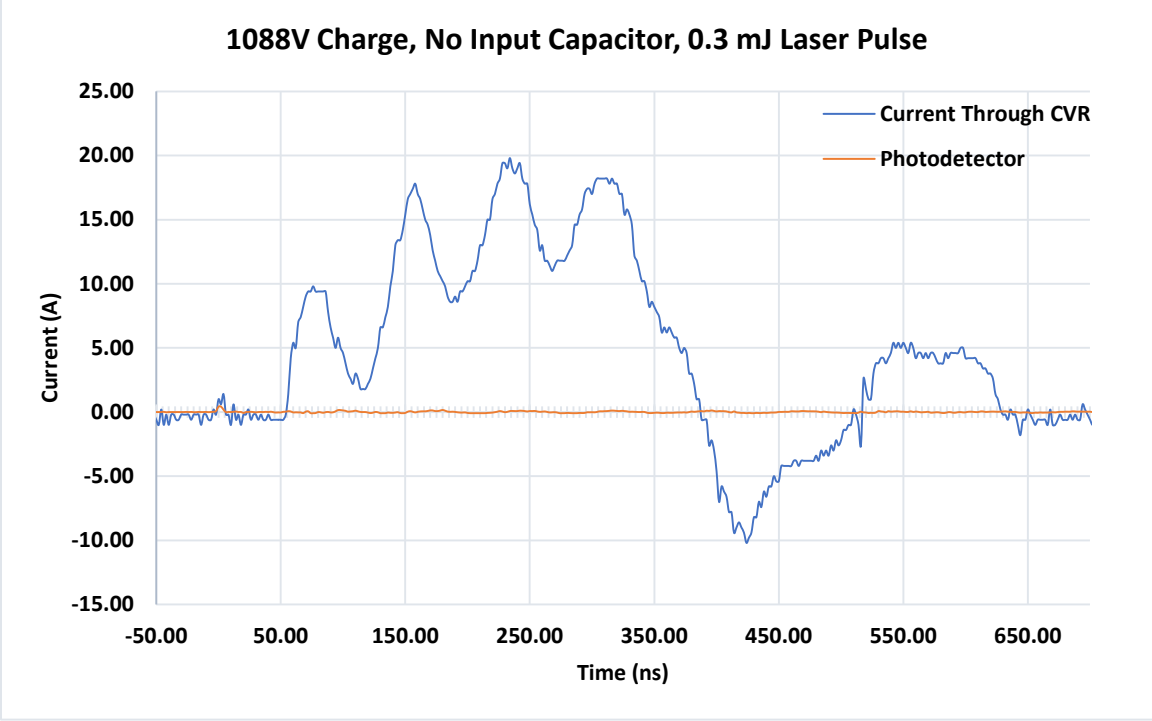

Figure 41: AMMONO GaN Nonlinear at 1088V, 0.3mJ laser pulse

Figure 42: AMMONO GaN filament at 1088V, 0.3mJ laser pulse

The 1500pF input capacitor was then added to further test the device. This was also taken as an opportunity to further optimize the imagery of the filaments. The previous test at 1100V nominal (1010V observed), 300μJ was then repeated (this time through a 2x attenuator due to the predicted increase in current) and 5x increase in current across the CVR, to 100A was observed.

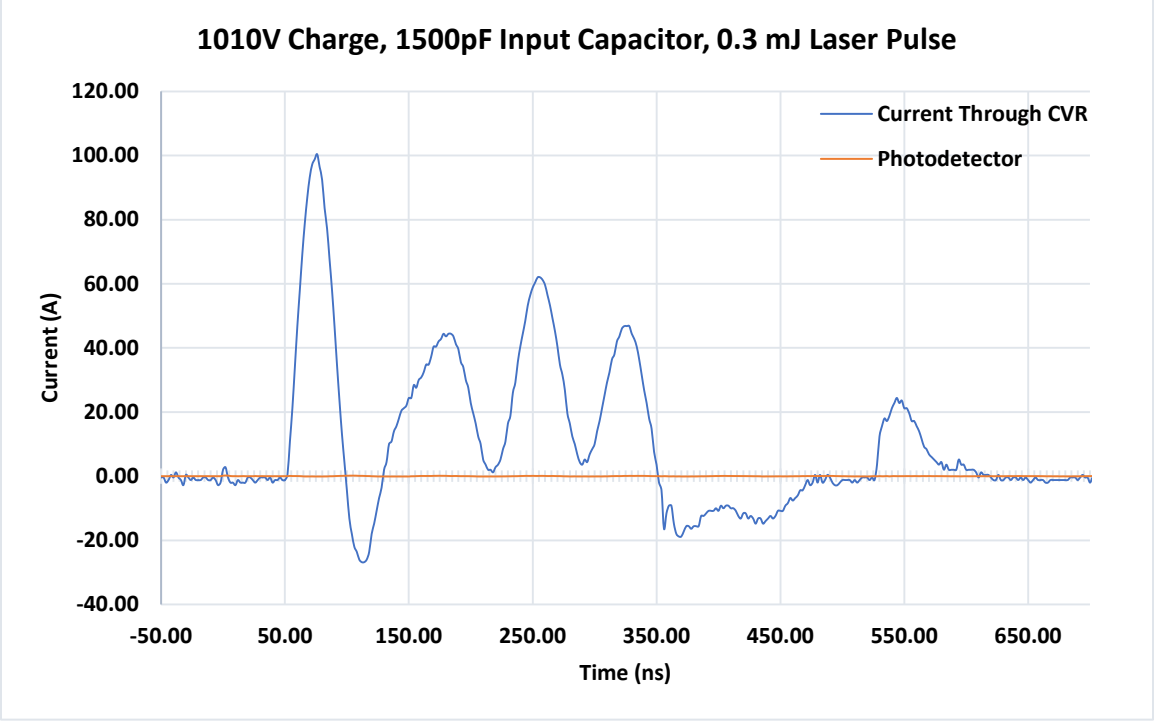

Figure 43: AMMONO GaN Nonlinear at 1010V, 0.3mJ laser pulse, 1500pF input capacitor, 2x attenuator

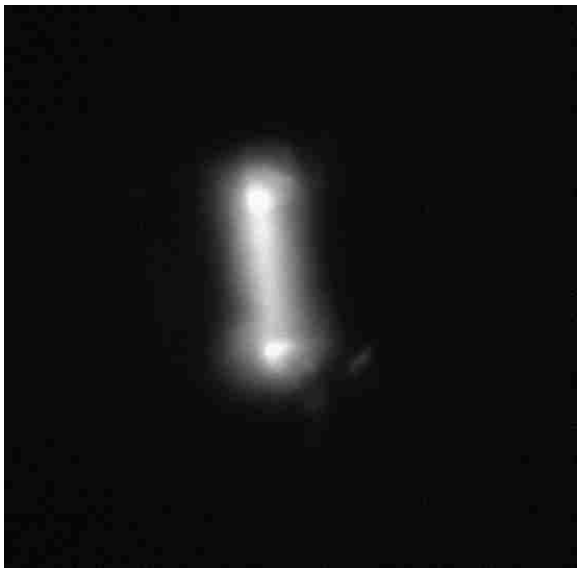

Figure 44: AMMONO GaN filament at 1010V, 0.3mJ laser pulse

After successfully testing at 1055V, 300μJ, and yielding 108A, as well as a double filament (Figure 45), it was decided to continue reducing laser energy to determine the minimum amount required for triggering. Testing was halted when a nonlinear response was triggered at 1104V (Figure 46, Figure 47), yielding 117A across the CVR with only 35μJ of laser energy. Because this was barely above the 15μJ background energy of the room measured with the laser power meter, obtaining meaningful results at lower power levels was unfeasible. Laser trigger energy vs field strength is shown in Table 7. For every kV increase in field strength, laser energy could be reduced by 166μJ.

Field Strength (kV/cm)	Trigger Energy (μJ)
16.8	300
17.6	92
18.4	35

Table 7: AMMONO GaN Field Strength vs Laser Energy

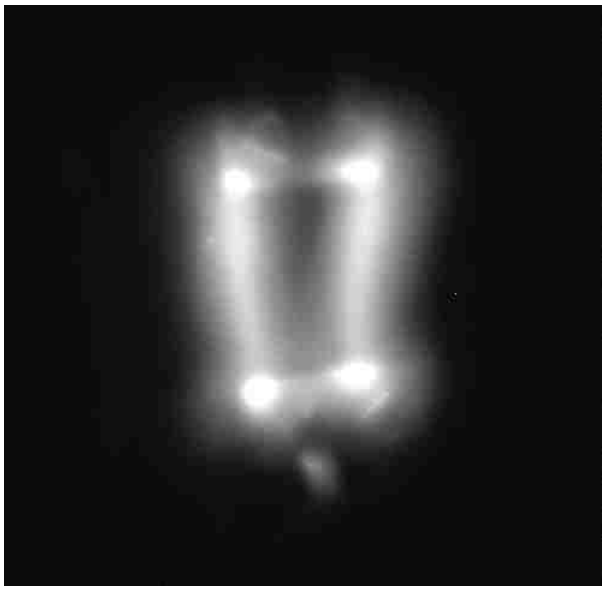

Figure 45: AMMONO GaN double filament at 1055V, 300μJ laser pulse, 1500pF input capacitor

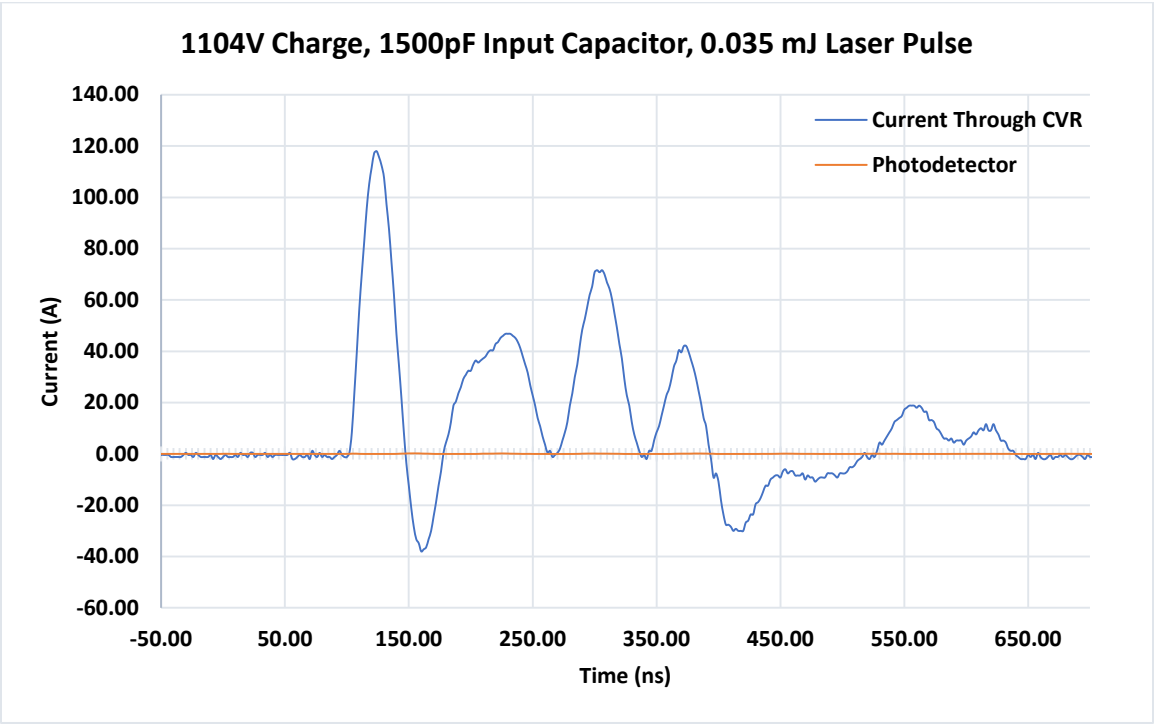

Figure 46: AMMONO GaN Nonlinear at 1104V, 35μJ laser pulse, 1500pF input capacitor, 2x attenuator

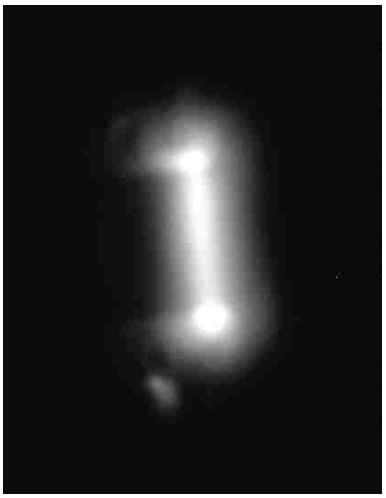

Figure 47: AMMONO GaN filament at 1104V, 35μJ laser pulse, 1500pF input capacitor, 2x attenuator

Having exhausted the lower bounds of the device, the next step was to see what would occur with a reasonable amount of light (2.7mJ) at a high field strength (1247V). This produced 131A (a shot power of 164kW), moved the nonlinear response closer to the linear one, and created filamentation across the breadth of the device, as can be seen in Figure 48 and Figure 49.

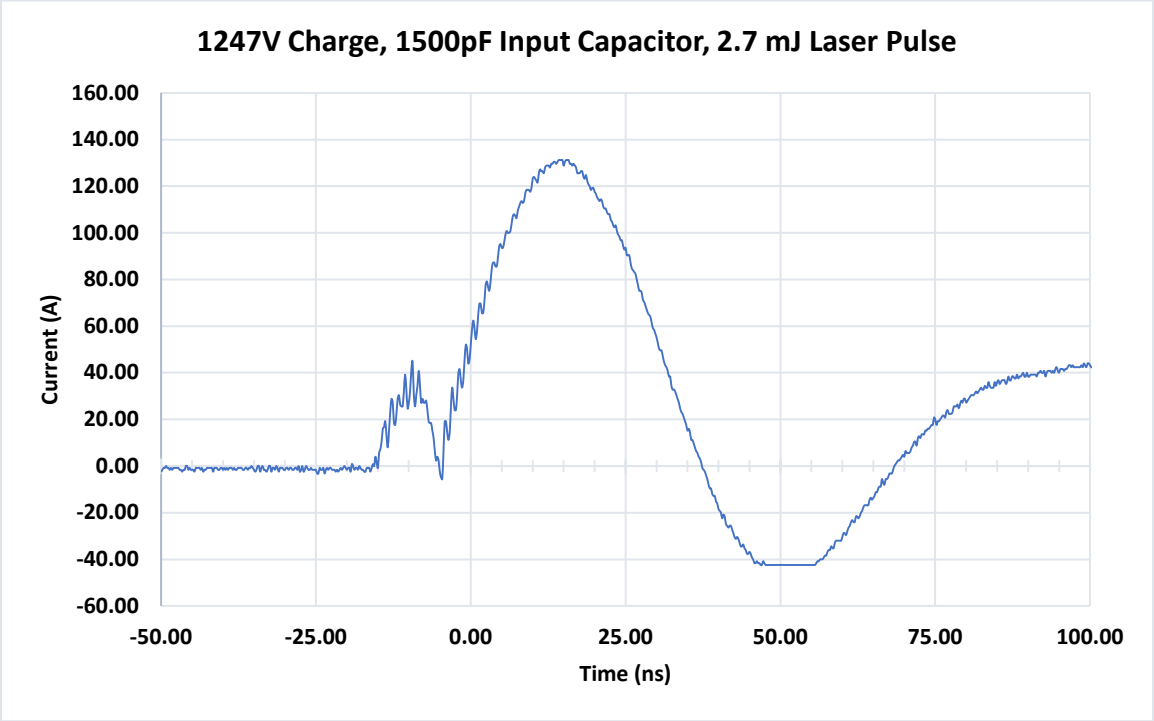

Figure 48: AMMONO GaN Nonlinear at 1247V, 2.7mJ laser pulse, 1500pF input capacitor, 2x attenuator

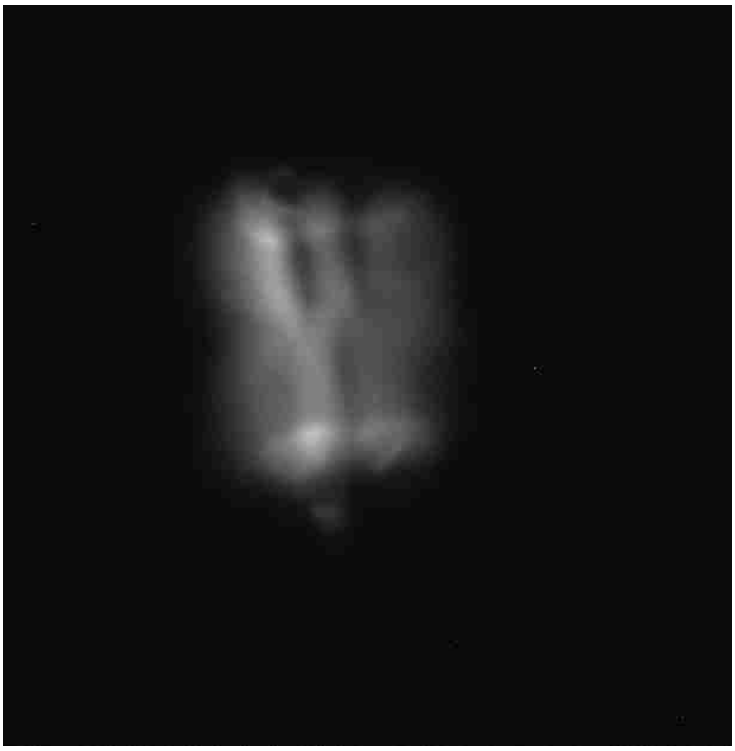

Figure 49: AMMONO GaN filaments at 1247V, 2.7mJ laser pulse, 1500pF input capacitor, 2x attenuator

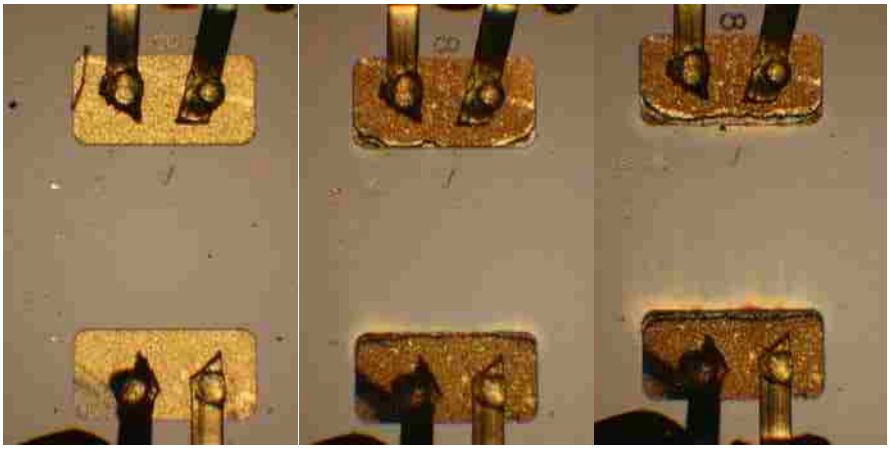

Figure 50: AMMONO devices after use

The AMMONO devices showed the best results yet in terms of durability. After 150 shots (including 50+ at powers greater than 100kW), the wear pattern across the fronts of the electrodes was nearly uniform, and no carbonization was observed. The rainbow effect was also less pronounced than on the Kyma devices. After this round of testing, the device was still functioning perfectly.

The AMMONO devices produced the most convincing evidence yet of a high-gain mode in GaN. They exhibited a strong nonlinear response below bandgap at very low laser pulse energies. Exceptional durability was demonstrated, and filament formation was non-preferential within the substrate, instead moving with the location of the laser beam. They were an excellent candidate for work in an oil bath to test higher field strengths without inducing surface flashover. In addition, their performance made a convincing argument for the creation of larger devices using the same material to produce higher power switches.

The devices still don't appear to form persistent channels with filament formation, at least not the way it occurs in GaAs. This is further supported by the variation in filament location from shot to shot. Characterization of the wavelength emitted by the filaments is also needed to determine their spectral characteristics and gain some insight into their source. An examination of device performance at shorter wavelengths (closer to bandgap energy), shorter pulse widths, and higher repetition rates (1kHz vs 1-10Hz) is also warranted and is recommended for future testing.

3.4: Overview of Results

Across three batches of devices from two separate sources of bulk material, GaN consistently demonstrated a nonlinear, high-gain mode of operation when triggered at 532nm. This is a world first. Additionally, it demonstrated these characteristics at relatively low field strengths and laser trigger energies while exhibiting exceptional durability, especially given the immaturity of the process used to create the devices. Damage to the devices was primarily at the contact pads, which could be mitigated

through better pad geometry, improved adhesion, and the immersion of the device in dielectric fluid. Table 8 gives a summary of the results and figures used in the body of this thesis but is merely a representative sample of the data collected during this project. Except for the Kyma Lot 1 device, which failed catastrophically, hundreds of shots were taken with each device, and shot-to-shot repeatability was so precise that the waveforms could be overlapped as shown below in Figure 51.

This repeatability also alleviated concerns that the phenomenon observed was surface flashover. Additional evidence that this was not flashover was that a.) the field strengths used were lower than the breakdown of air, and b.) filament location was influenced by beam location, as shown in Figure 40. Repeated tests were done, both blocking the beam while keeping the bias voltage high, and increasing the beam intensity while reducing bias voltage, to ensure that the phenomenon observed was not an artifact of either the laser intensity or the bias voltage, but rather a combination of both aspects. Device performance improved markedly above threshold voltage for a given laser energy, reducing jitter in both time and voltage domains, which matches previously observed behavior in GaAs PCSS devices.

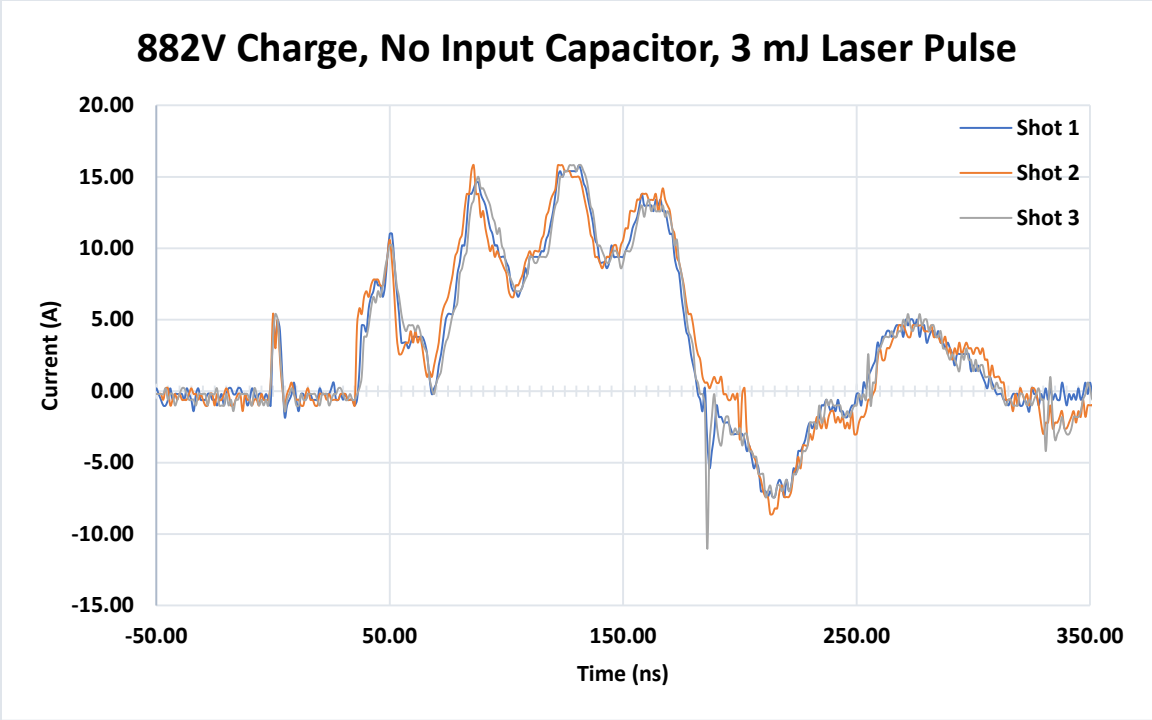

Figure 51: 3 shots at 883V in the AMMONO GaN device. Note the shot-shot repeatability.

Device	Capacitor	Field (V/cm)	Laser (mJ)	Voltage (V)	Current (A)	Mode	Power (kW)
Kyma Lot 1							
	N	0.00	8.00	0.00	0.01	Linear	0.00
	Y	8066.67	2.00	484.00	3.80	Linear	1.84
	N	16266.67	2.00	976.00	16.40	Nonlinear	16.01
	Y	8533.33	2.00	512.00	37.00	Nonlinear	18.94
	Y	12233.33	2.00	734.00	61.00	Nonlinear	44.77
Kyma Lot 3							
	N	2983.33	12.50	179.00	3.10	Linear	0.55
	N	10783.33	12.50	647.00	12.80	Nonlinear	8.28
	Y	10366.67	12.50	622.00	45.40	Nonlinear	28.24
	Y	19983.33	12.50	1199.00	107.00	Nonlinear	128.29
	Y	24266.67	12.50	1456.00	97.00	Nonlinear	141.2
AMMONO							
	N	3016.67	3.00	181.00	2.11	Linear	0.38
	N	14700.00	3.00	882.00	10.10	Nonlinear	8.91
	N	18133.33	0.30	1088.00	19.80	Nonlinear	21.54
	Y	16833.33	0.30	1010.00	100.04	Nonlinear	101.04
	Y	17583.33	0.30	1055.00	108.00	Nonlinear	113.94
	Y	18400.00	0.04	1104.00	117.00	Nonlinear	129.17
	Y	20783.33	2.70	1247.00	131.20	Nonlinear	163.61

Table 8: Overview of Results

Additionally, an accidental discovery was made during testing. While gathering spectral data, a miscommunication occurred, and a Hextech AlN PCSS device was left in the test setup. When spectral data was taken the next day, filament formation occurred in AlN, as can be seen in Figure 52, and proof of nonlinearity was also captured by the oscilloscope, as in Figure 53. However, it was decided to focus on GaN in the near-term, and thus the AlN devices have not been tested or characterized beyond what is shown below.

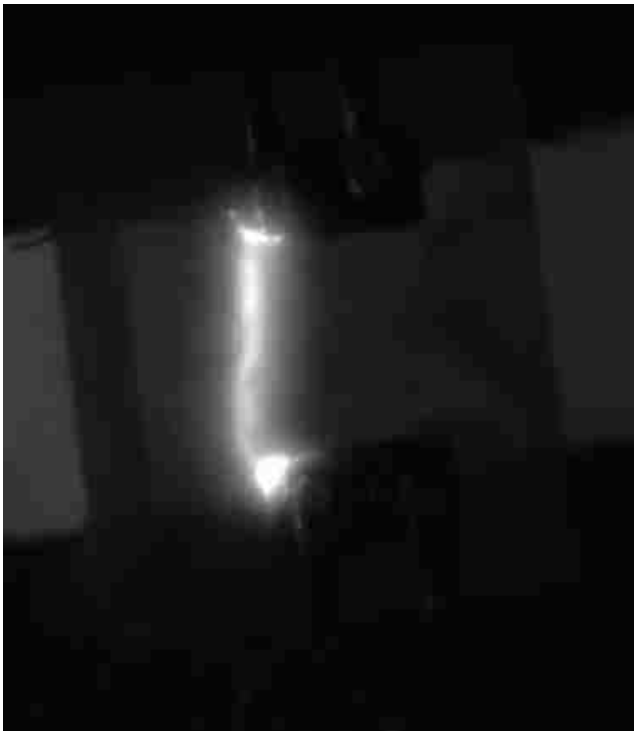

Figure 52: Hextech AlN filament at 1481V, 13mJ laser pulse

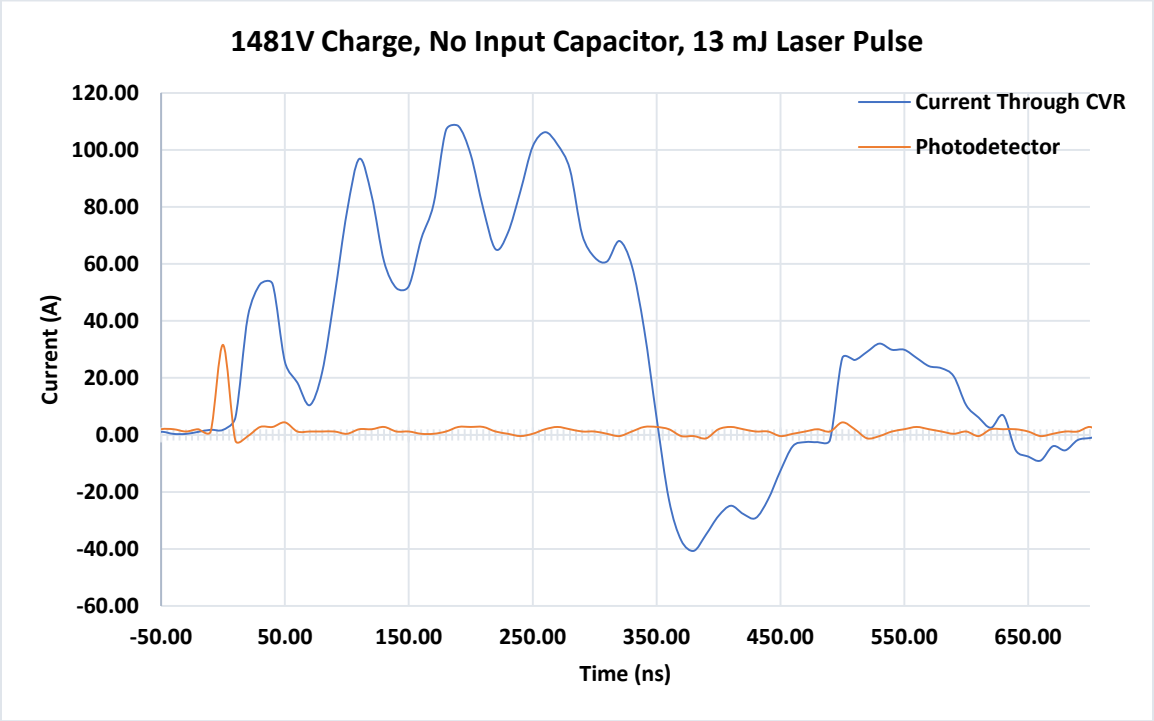

Figure 53: Hextech AlN Nonlinear at 1481V, 13mJ laser pulse

Chapter 4: Conclusions and Unanswered Questions

GaN possesses a previously undiscovered nonlinear, high-gain mode. This mode can be triggered sub-bandgap at 532nm, with ultra-low pulse energies (35uJ). Shot to shot consistency in resultant waveforms has also been demonstrated in both the time domain and amplitude/shape of the waveform itself, proving that this phenomenon is not surface flashover, which would be randomized in both aspects. Additionally, it appears that AlN may also possess a nonlinear, high-gain mode given preliminary results.

Device durability appears to be exceptional at first glance, with the majority of device degradation due to the experiments being performed in air, leading to damage to the electrodes, rather than the device substrate.

However, the noisiness of the results as well as the long (100ns) delays between linear and nonlinear operation at lower field strengths and optical energies demand a more rigorous investigation. This behavior is however consistent with that of GaAs PCSS based on extensive test experience the team has with GaAs. The ramifications of the multicolor streaking on device performance and lifetime are also unexplored. Future lifetime testing should help determine what, if any impact this “rainbow” effect has on device performance.

Presently it is unclear as to why this experiment showed evidence for nonlinear behavior when previous efforts did not. Nothing in the test setup was unusual or extreme relative to what others have tried. Laser pulse energies and durations, as well as electric field strengths were well within or below the ranges used by Meyers, Sullivan, or Kyma [5] [14] [24]. One hypothesis advanced by Dr. Alan Mar and Emily Hirsch, who manage

the ARPA-E GaN program, is that it may be a surface effect, and as such cannot be found in vertical devices or devices that have been potted or insulated, such as with dielectric fluid. Future testing is recommended to investigate this possibility.

4.1: Results of Further Efforts and Recommendations for Future Work

Efforts conducted by the team after the material presented in this thesis have shown time domain jitter on the order of 650ps, switching delays less than 5.5ns, and a lock-on field of 200V (3kV/cm) at trigger energies of 30μJ [27]. These results support and validate the material presented herein. The team also tested the devices under Fluorinert FC-70 and was unable to trigger a nonlinear mode of operation.

Additionally, it was decided to create larger devices, with 2mm spacing between electrodes in both the lateral configuration used for this thesis, as well as a vertical switch, to hopefully leverage the bulk properties of the material and achieve higher hold-off voltages without needing to resort to an oil bath.

Effort should also be expended on the modeling and simulation side, as field enhancement effects may have a substantial effect on device performance and triggering. The electrode modeling work by Meyers is of interest, as he posits that field enhancement effects could have a substantial impact on switching results.

The triple point interface of bulk GaN/electrode/dielectric may also have an impact on the mode of operation. One of the theories advanced by the team on this project is that the differing dielectric strengths of air compared to other common dielectric materials may be the reason other groups have not seen nonlinear behavior. All

devices tested previously have either been a vertical configuration or potted/insulated in some manner.

The optical interaction of the laser trigger with various dielectrics should also be explored. Other areas of interest would include: trigger polarization, trigger wavelength, trigger pulse width, trigger beam profile, and crystal orientation of the device.

References

[1] O. S. Zucker, K. Paul and Y.-M. Sheu, "GaN Switches in Pulsed Power: A Comparative Study," *IEEE Transactions on Plasma Science,* vol. 42, no. 5, pp. 1295-1303, 2014.

[2] G. Loubriel, "Photoconductive Semiconductor Switches," *IEEE Transactions on Plasma Science,* vol. 25, no. 2, pp. 124-130, 1997.

[3] C. Ruan, "Characteristic of the Ultra-Wideband Electromagnetic Radiation Generated by PCSS," *Microwave and Optical Technology Letters,* vol. 49, no. 5, pp. 1118-1122, 2007.

[4] "Electronics Coach," [Online]. Available: https://electronicscoach.com/material.html. [Accessed 19 07 2018].

[5] J. S. Sullivan, "Wide Bandgap Extrinsic Photoconductive Switches," Lawrence Livermore National Laboratory, 2013.

[6] E. Majda-Zdancewicz, "Current State of Photoconductive Semiconductor Switch Engineering," *Opto-Electronics Review,* vol. 26, pp. 92-102, 2018.

[7] G. M. Loubriel, "Photoconductive Semiconductor Switches: Laser Q-Switch Trigger and Switch-Trigger Laser Integration," Sandia National Laboratories, Albuquerque, NM, 1997.

[8] M. Bhatganar, "Comparison of 6H-SiC, 3C-SiC, and Si for Power Devices," *IEEE Transactions on Electron Devices,* vol. 40, no. 3, pp. 645-655, 1993.

[9] R. J. Kaplar, "Generation-After-Next Power electronics: Ultrawide-Bandgap Devices, High-temperature Packaging, and Magnetic Nanocomposite Materials," *IEEE Power Electronics Magazine,* vol. 4, no. 1, pp. 36-42, 2017.

[10] M. Schupbach, "High Power Density Silicon Carbide Power Electronic Converters," 29 September 2008. [Online]. Available: http://www.sandia.gov/ess/docs/pr_conferences/2008/schupbach_apei.pdf. [Accessed 23 April 2018].

[11] R. Nune, "Comparative Analysis of Power Density in Si MOSFET and GaN HEMT Based Flyback Converters," in *Proc. 10th Int. Conf. Compatability Power Electronics and Power Engineering*, 2016.

[12] R. Brown, A novel AlGaN/GaN based enhancement-mode high electron mobility transistor with sub-critical barrier thickness, Glasgow: University of Glasgow, 2015.

[13] X. Wang, "Saturability Algorithm of a Sub-Bandgap Laser for Triggering a Photoconductive Switch," *IEEE Journal of the Electron Devices Society,* vol. 5, no. 5, pp. 395-399, 2017.

[14] J. H. Leach, "High Voltage Bulk GaN-Based Photoconductive Switches for Pulsed Power Applications," in *Proc. SPIE 8625*, 2013.

[15] C. Honsberg, "Absorption Coefficient," [Online]. Available: https://www.pveducation.org/pvcdrom/absorption-coefficient. [Accessed 19 07 2018].

[16] X. Wang and S. K. Mazumder, "A Photoconductive Semiconductor Switch Vertically Embedded with MISFETs for High-Power High-Repitition-Rate Application," in *IEEE International Symposium on Power Electronics for Distributed Generation Systems (PEDG)*, Aachen, 2015.

[17] W. Shi, "30 kV and 3 kA Semi-Insulating GaAs Photoconductive Semiconductor Switch," *Applied Physics Letters*, vol. 92, no. 4, 2008.

[18] F. Zutavern, "High current, Multi-Filament Photoconductive Semiconductor Switching," in *IEEE Pulsed Power Conference*, Chicago, 2011.

[19] G. M. Loubriel, "High Current Photoconductive Semiconductor Switches," in *18th Power Modulator Symposium*, Hilton Head, SC, 1988.

[20] F. Zutavern, "Properties of High Gain GaAs Switches for Pulsed Power Applications," in *IEEE International Pulsed Power Conference*, 1997.

[21] G. Caporaso, "The Dielectric Wall Accelerator," Lawrence Livermore National Laboratory, 2009.

[22] Kyma Technologies, "kyma technologies," [Online]. Available: http://www.kymatech.com/. [Accessed 23 07 2018].

[23] AMMONO, "AMMONO," [Online]. Available: https://www.ammono.com/. [Accessed 23 07 2018].

[24] V. Meyers, "Toward the Development of an Efficient Bulk SemiInsulating GaN Photoconductive Switch," in *IEEE International Conference on Pulsed Power (PPC)*, 2017.

[25] H. Rahaman, "A Spark Gap Switch With Very High Repitition Rate," in *International Conference on Phenomena in Ionized Gases*, Prague, 2007.

[26] J. Lehr, Foundations of Pulsed Power Technology, Wiley-IEEE Press, 2017.

[27] A. Mar, "High-Gain Persistent Nonlinear Conductivity In High-Voltage Gallium Nitride Photoconductive Switches," in *2018 IEEE International Power Modulator and High Voltage Conference*, 2018.

[28] W. Shi, "Investigation of Electric Field Threshold of GaAs Photoconductive Semiconductor Switch Triggered by 1.6 uJ Laser Diode," *Applied Physics Letters*, vol. 104, no. 4, 2014.

[29] F. J. Zutavern, "Photoconductive Semiconductor Switch Experiments for Pulsed Power Applications," *IEEE Transactions on Electron Devices*, vol. 37, no. 12, pp. 2472-2477, 1990.

[30] C. Kittel, Introduction to Solid State Physics, John Wiley & Sons, Inc, 2005.

[31] J. S. Sullivan and J. R. Stanley, "Wide Bandgap Extrinsic Photoconductive Switches," *IEEE Transactions on Plasma Science*, vol. 36, no. 5, pp. 2528-2532, 2008.

[32] G. M. Loubriel, "Physics and Applications of the Lock-on Effect," Sandia National Laboratories, Albuquerque, 1991.